Eigenvalue Beamforming Using a Multirank MVDR Beamformer and Subspace Selection

Ali Pezeshki, *Member, IEEE*, Barry D. Van Veen, *Fellow, IEEE*, Louis L. Scharf, *Life Fellow, IEEE*, Henry Cox, *Life Fellow, IEEE*, and Magnus Lundberg Nordenvaad, *Member, IEEE*

***Abstract*—We derive *eigenvalue beamformers* to resolve an unknown signal of interest whose spatial signature lies in a known subspace, but whose orientation in that subspace is otherwise unknown. The unknown orientation may be fixed, in which case the signal covariance is rank-1, or it may be random, in which case the signal covariance is multirank. We present a systematic treatment of such signal models and explain their relevance for modeling signal uncertainties. We then present a multirank generalization of the MVDR beamformer. The idea is to minimize the power at the output of a matrix beamformer, while enforcing a data dependent distortionless constraint in the signal subspace, which we design based on the type of signal we wish to resolve. We show that the eigenvalues of an error covariance matrix are fundamental for resolving signals of interest. Signals with rank-1 covariances are resolved by the largest eigenvalues of the error covariance, while signals with multirank covariances are resolved by the smallest eigenvalues. Thus, the beamformers we design are eigenvalue beamformers, which extract signal information from eigenmodes of an error covariance. We address the tradeoff between angular resolution of eigenvalue beamformers and the fraction of the signal power they capture.**

***Index Terms*—Eigenvalue beamforming, generalized sidelobe canceller, matched direction beamforming, matched subspace beamforming, multirank MVDR beamformer.**

I. Introduction

In many applications of wireless communications, radar, sonar, and biomedical imaging, it is desired to separate a signal of interest in the presence of interference and noise using measurements from L sensor elements, e.g., see [1]. Typically, the problem is one of estimating a signal $s(t)$ in the measurement model

$$\mathbf{x}(t) = \mathbf{s}(t) + \boldsymbol{\nu}(t) + \mathbf{n}(t); \quad \mathbf{s}(t) = \mathbf{a}s(t) \tag{1}$$

where $\mathbf{a}$ is the spatial signature of interest, $\boldsymbol{\nu}(t)$ is the interference vector, and $\mathbf{n}(t)$ is broadband noise. When exact knowledge of the signature vector $\mathbf{a}$ is available, adaptive beamformers provide high spatial resolution and good interference suppression. However, in most situations the signature vector $\mathbf{a}$ is not perfectly known, due to factors such as multipath, local and random scattering, near field wavefront formation, random fluctuations in the propagation medium, array flexing, array calibration errors, and movement of the source. Differences between the presumed signature and the actual signature result in signal suppression and poor interference rejection [2]–[5].

To date several methods have been reported to account for uncertainty in the signature vector. A few examples are: the robust adaptive beamformers of [6], which enforce a white noise gain constraint; robust adaptive beamformers of [7], [8], which consider an ellipsoidal uncertainty for the signature vector; robust adaptive beamformers of [9] which optimize worst-case performance for a bounded norm distortion in the signature vector; robust adaptive beamformers of [10], which enforce a second-order distortionless constraint on a general rank signal covariance matrix; signal estimation methods of [11], [12], for the case where the unknown parameters of the signature vector are deterministic; and Bayesian approaches of [13], [14], for the case where the unknown parameters of the signature vector are randomly drawn from a known probability density. Other examples include the linearly constrained minimum variance (LCMV) beamformer in [15], Bayesian robust adaptive beamformer of [16], and signal blocking-based algorithms of [2], [17]. The reader is referred to [18] for a comprehensive review of the relevant literature.

In this paper, we derive *multirank* generalizations of the MVDR beamformer to resolve an unknown signal of interest. We assume that the signature vector $\mathbf{a}$ lies in a known linear subspace and consider three signal models. In the first model, the signal is assumed to lie in a known one-dimensional subspace and has a known rank-1 covariance matrix. This corresponds to the point source assumption in sensor array processing, where conventional adaptive beamformers have good and predictable performance. In the second and third models, however, we assume that the signal lies in a known multidimensional subspace, but the signal orientation within the subspace is otherwise unknown. The unknown orientation may be fixed over a sequence of experimental realizations, in which case the signal covariance matrix is rank-one. Or the unknown

Manuscript received September 22, 2006; revised September 11, 2007. The associate editor coordinating the review of this manuscript and approving it for publication was Prof. Alle-Jan van der Veen. This work is supported in part under ONR contracts N00014-04-1-0084 and N0014-00-C-0145, DARPA contracts FA9550-04-1-0371 and FA8750-05-2-0285, and NIH award 1R21EB005473.

A. Pezeshki is with the Program in Applied and Computational Mathematics, Princeton University, Princeton, NJ 08544 USA (e-mail: pezeshki@math.princeton.edu).

B. D. Van Veen is with the Department of Electrical and Computer Engineering, University of Wisconsin, Madison, WI 53706 USA (e-mail: vanveen@engr.wisc.edu).

L. L. Scharf is with the Department of Electrical and Computer Engineering and the Department of Statistics, Colorado State University, Fort Collins, CO 80523 USA (e-mail: scharf@engr.colostate.edu).

H. Cox is with Lockheed Martin-Orincon Defense, Arlington, VA 22203 USA (e-mail: harry.cox@lmco.com).

M. Lundberg Nordenvaad is with the Department of Computer Science and Electrical Engineering, Luleå University of Technology, Luleå, Sweden (e-mail: mlg@sm.luth.se).

Digital Object Identifier 10.1109/TSP.2007.912248

orientation may change from realization to realization, in which case the signal covariance is multirank. The former can be used to model signals in the presence of slow-varying multipath, array calibration errors, and deterministic uncertainties about the relative source/sensor array geometry. The latter can be used to model signals in the presence of fast-varying multipath, local and random scattering, flexing arrays, and random uncertainties about the relative source/sensor array geometry. Conventional beamformers suffer loss in detectability and resolution, due to model mismatch, for both of these models.

We begin by presenting a unified and systematic treatment of our signal models and explain the rationale and relevance of such models for problems in radar, sonar, wireless communications, and biomedical imaging. This unified framework motivates the design and use of multirank beamformers as a general tool for robust adaptive beamforming in many real-life applications. We then present a multirank generalization of the MVDR beamformer. The idea is to minimize the power at the output of a *matrix* beamformer $\mathbf{W}$, while enforcing a *data dependent* distortionless constraint in the signal subspace. More specifically, we enforce a constraint of the form $\mathbf{W}^H\mathbf{\Psi} = \mathbf{Q}^H$, where $\mathbf{\Psi}$ is an orthonormal basis for the signal subspace and $\mathbf{Q}$ is a data dependent constraint matrix, which we design based on the type of signal we wish to resolve. We note that minimizing the power at the output of a matrix beamformer/filter under a constraint in a linear subspace has been considered before in [19] and [20]. Such a problem has also been considered in [21], but in the context of spectrum estimation. What distinguishes the multirank beamformers to be presented in this paper is that in [19]–[21] the desired response $\mathbf{Q}^H$ is prespecified (namely $\mathbf{Q} = \mathbf{I}$), whereas in our work the constraint matrix $\mathbf{Q}$ is a *data dependent design parameter*. The design of $\mathbf{Q}$ has important and surprising implications for resolving signals in the presence of model uncertainties. Incidentally, when $\mathbf{W}$ and $\mathbf{Q}$ are vectors the constraint $\mathbf{W}^H\mathbf{\Psi} = \mathbf{Q}^H$ reduces in form to the constraint of a Frost beamformer [22]. However, in the Frost beamformer the constraint vector is again prespecified. Our multirank beamformers are also related to the minimum variance CDMA receivers of [23], [24], the biomagnetic spatial filters of [25], and the robust adaptive beamformers of [10].

The critical quantities for resolving signals that are drawn from a multidimensional subspace are eigenvalues of an error covariance matrix, $\mathbf{R}_{ee}$, associated with the linear minimum mean-squared error (LMMSE) in a generalized sidelobe canceller (GSC). Although the GSC [26] is not necessary for implementing our beamformers, it is essential for understanding and interpreting multirank MVDR beamforming. We show that signals with rank-1 covariances are resolved by the dominant eigenvalues of $\mathbf{R}_{ee}$, while signals with multirank covariances are resolved by the subdominant eigenvalues of $\mathbf{R}_{ee}$. In the former case, the constraint matrix $\mathbf{Q}$ is selected to exploit the dominant eigenvectors of $\mathbf{R}_{ee}$. In the latter case, $\mathbf{Q}$ is selected to exploit the subdominant eigenvectors of $\mathbf{R}_{ee}$. This is a fundamental and surprising result. It shows that the dominant subspace of $\mathbf{R}_{ee}$ is fundamental for resolving signals with rank-1 covariances, or equivalently for beamforming in the presence of deterministic uncertainties. On the other hand, the subdominant subspace of $\mathbf{R}_{ee}$ is fundamental for resolving multirank signals, or equivalently for beamforming in the presence of random uncertainties with known second-order statistics. We call the multirank beamformers that resolve signals with rank-1 covariances *matched direction beamformers* and the multirank beamformers that resolve signals with multirank covariances *matched subspace beamformers*. Our use of language, and view of matched direction and matched subspace scenarios, is consistent with the use in [27]–[31], where matched direction detectors and matched subspace detectors are developed.

More importantly, we show that matched direction and matched subspace beamformers consist of a collection of *eigenvalue beamformers*, where each eigenvalue beamformer extracts a fraction of the signal power from an eigenmode of $\mathbf{R}_{ee}$. A multirank beamformer *diversity combines* a set of eigenvalue beamformers (dominant or subdominant) to capture a larger fraction of the signal power. We show that there exists a tradeoff between the fraction of the signal power captured at the multirank beamformer output and the angular resolution of the beamformer. The eigenvalue beamformer associated with the most dominant eigenvalue of $\mathbf{R}_{ee}$ offers the best angular resolution for resolving signals with rank-1 covariances. On the other hand, the best angular resolution for resolving signals with multirank covariances is provided by the eigenvalue beamformer corresponding to the most subdominant eigenvalue of $\mathbf{R}_{ee}$. Hence, eigenvalue beamformers are fundamental for resolving signals that are drawn from a multidimensional subspace, as each eigenvalue beamformer extracts signal information from an orthogonal subspace mode of the error covariance matrix and has an eigenvalue-dependent resolution. Numerical examples presented in Section VI demonstrate the key role of eigenvalues of $\mathbf{R}_{ee}$ in resolving signals of interest. Finally, we note that preliminary versions of this paper were reported in [32]–[34].

II. Signal Models

Consider the general L-dimensional data model $\mathbf{x} = \mathbf{s} + \boldsymbol{\nu} + \mathbf{n}$, consisting of a signal of interest $\mathbf{s} \in \mathbb{C}^L$ plus interference $\boldsymbol{\nu} \in \mathbb{C}^L$ and noise $\mathbf{n} \in \mathbb{C}^L$. Assuming that $\mathbf{s}$, $\mathbf{v}$, and $\mathbf{n}$ are uncorrelated and have zero means, we may express the measurement covariance matrix as

$$\mathbf{R} = E[\mathbf{x}\mathbf{x}^H] = \mathbf{R}_{ss} + \mathbf{R}_{\nu\nu} + \mathbf{R}_{nn} \tag{2}$$

where $\mathbf{R}_{ss} = \mathbf{E}[\mathbf{s}\mathbf{s}^H]$ is the signal covariance, $\mathbf{R}_{\nu\nu} = \mathbf{E}[\boldsymbol{\nu}\boldsymbol{\nu}^H]$ is the interference covariance, and $\mathbf{R}_{nn} = \mathbf{E}[\mathbf{n}\mathbf{n}^H] = \sigma_n^2\mathbf{I}$ is the noise covariance. We assume that the signal $\mathbf{s}$ lies in a linear subspace and consider the three following signal models.

Model 1: Sequence of signals with a rank-1 covariance from a known one-dimensional subspace. The signal $\mathbf{s}$ is modeled as

$$\mathbf{s} = \boldsymbol{\psi}s \tag{3}$$

where $\boldsymbol{\psi} \in \mathbb{C}^L$ is a known unit-norm vector, characterizing a known one-dimensional signal subspace $\langle\boldsymbol{\psi}\rangle$, and s is a zero-mean random complex amplitude with variance $\sigma_s^2 = E[ss^\star]$. In this case, the signal $\mathbf{s}$ has a rank-1 covariance matrix of the form

$$\mathbf{R}_{ss} = E[\mathbf{s}\mathbf{s}^H] = \sigma_s^2\boldsymbol{\psi}\boldsymbol{\psi}^H. \tag{4}$$

Realizations of $\mathbf{s}$ are generated by randomly drawing realizations of the complex amplitude s, and a sequence of N such realizations $\{\mathbf{s}[i] = \boldsymbol{\psi}s[i]\}_{i=1}^N$ produces a rank-1 experimental (sample) covariance matrix. All realizations of $\mathbf{s}$ lie in the known

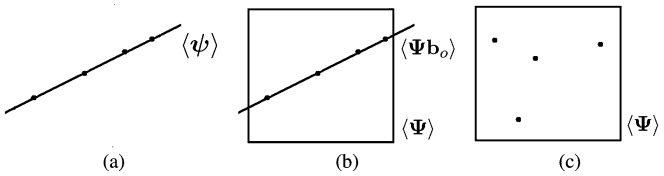

Fig. 1. (a) Realizations of a signal from a known one-dimensional subspace; (b) realizations of a signal from an unknown one-dimensional subspace within a known p-dimensional subspace; and (c) realizations of a signal from a known p-dimensional subspace.

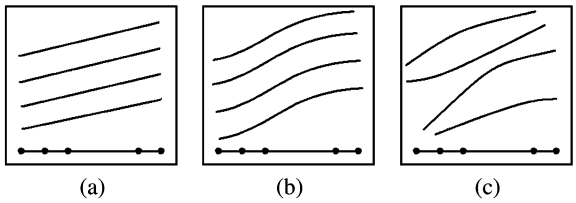

Fig. 2. (a) Standing waves drawn from (3), (b) standing waves drawn from (5), and (c) fluctuating waves drawn from (7).

one-dimensional subspace (or on the line) $\langle \boldsymbol{\psi} \rangle$, as illustrated in Fig. 1(a). Each dot on the line $\langle \boldsymbol{\psi} \rangle$ depicts a realization $\mathbf{s}[i] = \boldsymbol{\psi} s[i]$, $i = 1, \ldots, N$.

*Model 2: Sequence of signals with a rank-1 covariance from a known p-dimensional subspace.*The signal model is

$$\mathbf{s} = \boldsymbol{\Psi} \mathbf{b}_o s \tag{5}$$

where $\boldsymbol{\Psi}$ is a known $L \times p$ $(p < L)$ matrix with orthonormal columns $\left(\boldsymbol{\Psi}^H \boldsymbol{\Psi} = \mathbf{I}_{p \times p}\right)$, spanning a p-dimensional subspace $\langle \boldsymbol{\Psi} \rangle$. The vector $\mathbf{b}_o$ is an *unknown but fixed* $p \times 1$ unit-norm complex vector that determines the orientation of the signal $\mathbf{s}$ in $\langle \boldsymbol{\Psi} \rangle$, and s is a zero-mean random complex amplitude with variance σ_s^2. Here, the signal $\mathbf{s}$ is known to lie inside the p-dimensional subspace $\langle \boldsymbol{\Psi} \rangle$ but the coordinates of $\mathbf{s}$ in $\langle \boldsymbol{\Psi} \rangle$ are unknown. The signal $\mathbf{s}$ has a rank-1 but unknown covariance matrix of the form

$$\mathbf{R}_{ss} = E[\mathbf{s}\mathbf{s}^H] = \sigma_s^2 \boldsymbol{\Psi} \mathbf{b}_o \mathbf{b}_o^H \boldsymbol{\Psi}^H. \tag{6}$$

Realizations of $\mathbf{s}$ are generated by randomly drawing realizations of the complex amplitude s, and a sequence of N such realizations $\{\mathbf{s}[i] = \boldsymbol{\Psi} \mathbf{b}_o s[i]\}_{i=1}^N$ produces a rank-1 experimental covariance matrix. All realizations of $\mathbf{s}$ lie on the unknown line $\langle \boldsymbol{\Psi} \mathbf{b}_o \rangle$ inside the known p-dimensional subspace $\langle \boldsymbol{\Psi} \rangle$, as illustrated in Fig. 1(b).

Model 3: Sequence of signals with a rank-p covariance from a known p-dimensional subspace. The signal $\mathbf{s}$ is modeled as

$$\mathbf{s} = \boldsymbol{\Psi} \mathbf{b} s \tag{7}$$

where $\boldsymbol{\Psi}$ is a known $L \times p$ $(p < L)$ matrix with orthonormal columns, spanning a p-dimensional subspace $\langle \boldsymbol{\Psi} \rangle$. The vector $\mathbf{b}$ is a $p \times 1$ zero-mean complex random vector with a known rank-p covariance $\mathbf{R}_{bb} = E[\mathbf{b}\mathbf{b}^H]$, normalized so that $\mathrm{tr}\{\mathbf{R}_{bb}\} = 1$, and s is a random complex amplitude with variance σ_s^2 independent of $\mathbf{b}$. Here the signal $\mathbf{s}$ has a known rank-p covariance matrix of the form

$$\mathbf{R}_{ss} = E[\mathbf{s}\mathbf{s}^H] = \sigma_s^2 \boldsymbol{\Psi} \mathbf{R}_{bb} \boldsymbol{\Psi}^H. \tag{8}$$

Realizations of $\mathbf{s}$ are generated by randomly drawing realizations of both the orientation vector $\mathbf{b}$ and the complex amplitude s, and a sequence of N such realizations $\{\mathbf{s}[i] = \boldsymbol{\Psi} \mathbf{b}[i] s[i]\}_{i=1}^N$ produces a rank-p experimental covariance matrix. Each realization of $\mathbf{s}$ is built from a different linear combination of the columns of $\boldsymbol{\Psi}$ and produces a different point in the subspace $\langle \boldsymbol{\Psi} \rangle$, as illustrated in Fig. 1(c).

The three signal models introduced here capture a wealth of effects in radar, sonar, wireless communications, and biomedical imaging, as we describe in the remainder of this section.

A. Radar and Sonar

Let $\mathbf{h}(\phi, \omega)$ be the $L \times 1$ unit-norm bearing vector that carries the relative phases and amplitudes induced on the array elements due to a source radiating from angle ϕ at frequency ω. Depending on one's assumptions about the mechanism that generates $\mathbf{h}(\phi, \omega)$, the wavefront $\mathbf{s} = \mathbf{h}(\phi, \omega) s$ may be modeled as (3), (5), or (7) as we now show.

Case 1: Standing waves from a known one-dimensional subspace: If $\phi = \phi_o$ and $\omega = \omega_o$, then $\mathbf{s} = \mathbf{h}(\phi_o, \omega_o) s$ may be expressed as in (3) by setting $\boldsymbol{\psi} = \mathbf{h}(\phi_o, \omega_o)$. This is the typical point source model in sensor array processing. The relative phasings and amplitudes induced by the signal on the array elements do not vary from snapshot to snapshot, as all realizations of $\mathbf{s}$ are built from the fixed bearing vector $\boldsymbol{\psi} = \mathbf{h}(\phi_o, \omega_o)$. The name standing waves indicates that all the wavefronts in the sequence arrive from the same angle and have the same frequency. This is illustrated in Fig. 2(a) for the case of a uniform linear array (ULA), where each realization of $\mathbf{s}$ is a plane wave. In this figure, the straight line depicts the ULA and the oblique lines depict a sequence of plane waves, which maintain their angle of arrival and frequency over time. The only aspect that changes from one realization to another is the complex amplitude s along the wavefronts.

Case 2: Standing waves from a known p-dimensional subspace: Several scenarios in radar and sonar give rise to the signal model (5). In a multipath propagation scenario the signal $\mathbf{s}$ is a superposition of waves arriving from different angles (paths), all with the fixed frequency $\omega = \omega_o$, where each path has a complex gain associated with a scattering object. Suppose the arriving angles $\phi_1, \ldots, \phi_p$ are known, or are quantized, and the corresponding path gains $c(\phi_1), \ldots, c(\phi_p)$ are unknown but fixed, as in the case of slow-varying multipath during an observation period. Then, $\mathbf{s}$ can be expressed as $\mathbf{s} = \mathbf{H}\mathbf{c}_o \alpha$, where $\mathbf{H} = [\mathbf{h}(\phi_1, \omega_o), \ldots, \mathbf{h}(\phi_p, \omega_o)]$, $\mathbf{c}_o = [c(\phi_1), \ldots, c(\phi_p)]^T$, and α is a zero-mean random complex amplitude. If we decompose $\mathbf{H}$ as $\mathbf{H} = \boldsymbol{\Psi}\mathbf{F}$, where $\boldsymbol{\Psi}$ is an $L \times p$ orthonormal basis for $\langle \mathbf{H} \rangle$, we may then express $\mathbf{s}$ as in (5) by defining $\mathbf{b}_o = \mathbf{F}\mathbf{c}_o / \|\mathbf{F}\mathbf{c}_o\|_2$ and $s = \|\mathbf{F}\mathbf{c}_o\|_2 \alpha$.

The relative phasings and amplitudes induced by the signal on the array elements do not vary from snapshot to snapshot, as all realizations of $\mathbf{s}$ are built from the same linear combination of the columns of $\boldsymbol{\Psi}$. The name standing waves indicates that all

wavefronts in the sequence have the same "shape". This is illustrated in Fig. 2(b) for the case of a ULA, where each realization of $\mathbf{s}$ is a "wrinkled" or nonplane wave, but the wrinkling does not change from realization to realization.

If the source is broadband with fixed but unknown discrete spectrum on frequency band Ω_o, but arrives from a fixed and known angle $\phi = \phi_o$, we may use the DTFT to express $\mathbf{s}$ as $\mathbf{s} = \sum_{i=1}^{p} \mathbf{h}(\phi_o, \omega_i) c(\omega_i)\alpha = \mathbf{H}\mathbf{c}_o s$, where the ω_i, $i = 1, \ldots, p$ are the DTFT frequencies spanning Ω_o, $c(\omega_i)$ is the unknown but fixed source spectral content at frequency ω_i, $\mathbf{c}_o = [c(\omega_1), \ldots, c(\omega_p)]^T$, $\mathbf{H} = [\mathbf{h}(\phi_o, \omega_i), \ldots, \mathbf{h}(\phi_o, \omega_p)]$, and α is a zero-mean random complex amplitude. Since columns of the DTFT matrix $\mathbf{H}$ are orthonormal we may express $\mathbf{s}$ in the form of (5) by defining $\mathbf{\Psi} = \mathbf{H}$, $\mathbf{b}_o = \mathbf{c}_o / \|\mathbf{c}_o\|_2$ and $s = \|\mathbf{c}_o\|_2 \alpha$.

The model (5) is also applicable when there is deterministic uncertainty about the bearing vector, due to array calibration errors. Let γ denote the uncertainty in the parameters of the bearing vector associated with the signal wavefront, so $\mathbf{s} = \mathbf{h}(\gamma)s$, and assume that γ is fixed and known to lie in the interval $\Gamma = [\gamma_o - \Delta\gamma, \gamma_o + \Delta\gamma]$. Let γ_i, $i = 1, \ldots, K$ be a sampling of Γ and define $\mathbf{H} = [\mathbf{h}(\gamma_1), \ldots, \mathbf{h}(\gamma_K)]$. If the sampling is sufficiently dense, then the true but unknown $\mathbf{h}(\gamma)$ may be represented as a linear combination of adjacent columns of $\mathbf{H}$. Let $\mathbf{\Psi}$ be the $L \times p$ matrix whose columns are the first p left singular vectors of $\mathbf{H}$, where p is the numerical rank of $\mathbf{H}$. Then, $\mathbf{h}(\gamma)$ approximately lies in $\langle \mathbf{\Psi} \rangle$, so we may approximate $\mathbf{s}$ as $\mathbf{s} = \mathbf{\Psi}\mathbf{b}_o s$, where $\mathbf{b}_o$ is a $p \times 1$ unknown but fixed vector of complex coefficients.

Case 3: Fluctuating waves from a known p-dimensional subspace: We now consider a few scenarios which give rise to the signal model in (7). Consider a narrowband ($\omega = \omega_o$) but spatially distributed source which radiates with angular power density $S(\phi)$, from a continuum of angles $\Phi = [\phi_o - \Delta\phi, \phi_o + \Delta\phi]$. The covariance matrix for the source is given by

$$\mathbf{R}_{ss} = E[\mathbf{s}\mathbf{s}^H] = \sigma_s^2 \int_{\phi_o - \Delta\phi}^{\phi_o + \Delta\phi} \mathbf{h}(\phi, \omega_o)\mathbf{h}^H(\phi, \omega_o) dS(\phi). \tag{9}$$

For sufficiently small $\Delta\phi$, $\mathbf{R}_{ss}$ is numerically rank deficient. Thus, we may approximate $\mathbf{R}_{ss}$ with the rank-p eigendecomposition $\mathbf{R}_{ss} = \sigma_s^2 \mathbf{\Psi}\mathbf{\Lambda}\mathbf{\Psi}^H$, where p is the numerical rank of $\mathbf{R}_{ss}$, $\mathbf{\Lambda} = \mathrm{diag}\{\lambda_1, \ldots, \lambda_p\}$ contains the p largest eigenvalues of $(1/\sigma_s^2)\mathbf{R}_{ss}$, with $\sigma_s^2 = \mathrm{tr}\{\mathbf{R}_{ss}\}$, and $\mathbf{\Psi} \in \mathbb{C}^{L \times p}$ contains the corresponding eigenvectors. Consequently, a distributed source $\mathbf{s}$ with known covariance $\mathbf{R}_{ss} = \sigma_s^2 \mathbf{\Psi}\mathbf{\Lambda}\mathbf{\Psi}^H$ may be modeled as in (7), provided that the orientation vector $\mathbf{b}$ is randomly drawn from a distribution with known covariance $\mathbf{R}_{bb} = E[\mathbf{b}\mathbf{b}^H] = \mathbf{\Lambda}$, and the complex amplitude s is independently drawn from a distribution with variance $\sigma_s^2 = \mathrm{tr}\{\mathbf{R}_{ss}\}$.

The relative phasings and amplitudes induced by the signal on the array elements vary from snapshot to snapshot, as each realization of $\mathbf{s}$ is built from a different linear combination of the columns of $\mathbf{\Psi}$. The name fluctuating waves indicates that each wavefront in the sequence will have a different shape. This is illustrated in Fig. 2(c) for the case of a ULA, where each realization of $\mathbf{s}$ is a wrinkled wave, but the wrinkling changes from one realization to another.

Remark 1: If the array is an L-element ULA with half-wavelength inter-element spacings and the angular power density $S(\phi) = 1/(2\Delta\phi)$ is uniform on the angular bandwidth Φ, then the approximate numerical rank of $\mathbf{R}_{ss}$ is $p = (\Delta\phi/\pi)L = \beta L$, where $0 \leq \beta = (\Delta\phi/\pi) < 1$ is called the fractional wavenumber bandwidth, and $\mathbf{\Lambda}$ is approximated as $\mathbf{\Lambda} = (1/p)\mathbf{I}$. The columns of $\mathbf{\Psi}$ are the first p discrete prolate spheroidal wave functions and $\langle \mathbf{\Psi} \rangle$ is the corresponding p-dimensional *Slepian subspace* [35]–[37].

Similarly, a broadband source at a fixed angle $\phi = \phi_o$ with power spectral density $S(w)$ on the frequency band $\Omega_o = [\omega_o - \Delta\omega, \omega_o + \Delta\omega]$ may be modeled as in (7). The signal covariance $\mathbf{R}_{ss}$ is of the form (9), with ω playing the role of ϕ. The numerical rank of $\mathbf{R}_{ss}$ is given by the time-bandwidth product $T\Delta\omega$, where T is the transmit time of the wavefront across the array and is thus a function of ϕ_o [38]. Hence, we may use the rank-p eigendecomposition $\mathbf{R}_{ss} = \sigma_s^2 \mathbf{\Psi}\mathbf{\Lambda}\mathbf{\Psi}^H$ and model $\mathbf{s}$ as in (7).

The model (7) is also applicable when the uncertainty γ in the bearing vector changes randomly during the observation interval, e.g., due to flexing of a towed array in sonar. Suppose γ is drawn randomly from a distribution $F(\gamma)$ over $\Gamma = [\gamma_o - \Delta\gamma, \gamma_o + \Delta\gamma]$. Then, the signal covariance matrix $\mathbf{R}_{ss} = E[\mathbf{s}\mathbf{s}^H]$ is[1]

$$\mathbf{R}_{ss} = E[\mathbf{s}\mathbf{s}^H] = \sigma_s^2 \int_{\gamma_o - \Delta\gamma}^{\gamma_o + \Delta\gamma} \mathbf{h}(\gamma)\mathbf{h}^H(\gamma) dF(\gamma). \tag{10}$$

If we take the numerical rank of $\mathbf{R}_{ss}$ to be p, then $\mathbf{R}_{ss}$ may be approximated by a rank-p eigendecomposition $\mathbf{R}_{ss} = \sigma_s^2 \mathbf{\Psi}\mathbf{\Lambda}\mathbf{\Psi}^H$. Therefore, we may again express $\mathbf{s} = \mathbf{h}(\gamma)s$ as $\mathbf{s} = \mathbf{\Psi}\mathbf{b}s$, where the random change of γ from realization to realization is modeled by the p-dimensional zero-mean random vector $\mathbf{b}$ with known covariance $\mathbf{R}_{bb} = E[\mathbf{b}\mathbf{b}^H] = \mathbf{\Lambda}$. In general, the numerical rank of $\mathbf{R}_{ss}$ increases as the support of $F(\gamma)$ increases.

B. Communications

Signal models (3), (5), and (7) are applicable to communication with a known code over a channel modeled as a p-tap FIR filter. Let $\mathbf{H}$ be an $L \times p$ matrix whose columns are the p time shifts of the length L code and let $\mathbf{m}$ be the $p \times 1$ vector of channel coefficients. Then, the received signal is of the form $\mathbf{s} = \mathbf{H}\mathbf{m}\alpha$, where α denotes the transmitted bit or amplitude. If $\mathbf{m}$ is assumed to be known from pilot symbols, then $\mathbf{s}$ may be written as (3) by defining $\boldsymbol{\psi} = \mathbf{H}\mathbf{m}/\|\mathbf{H}\mathbf{m}\|_2$ and $s = \|\mathbf{H}\mathbf{m}\|_2 \alpha$. If $\mathbf{m}$ is unknown but fixed, we may decompose $\mathbf{H}$ as $\mathbf{H} = \mathbf{\Psi}\mathbf{F}$, where $\mathbf{\Psi}$ is an orthonormal basis for $\langle \mathbf{H} \rangle$, and then write $\mathbf{s}$ as in (5) by defining $\mathbf{b}_o = \mathbf{F}\mathbf{m}/\|\mathbf{F}\mathbf{m}\|_2$ and $s = \|\mathbf{F}\mathbf{m}\|_2 \alpha$. Finally, if $\mathbf{m}$ is assumed to be random with known covariance $\mathbf{R}_{mm} = E[\mathbf{m}\mathbf{m}^H]$, then we may express $\mathbf{s}$ as in (7) by defining $\mathbf{b} = \mathbf{F}\mathbf{m}/E[\mathbf{m}^H\mathbf{F}^H\mathbf{F}\mathbf{m}]$ and $s = E[\mathbf{m}^H\mathbf{F}^H\mathbf{F}\mathbf{m}]\alpha$.

[1]Provided that the variance of γ is small, (10) may be approximated by a *coherence loss model* of the form $\mathbf{R}_{ss} = \sigma_s^2 \mathbf{h}(\gamma)\mathbf{h}^H(\gamma) \odot \mathbf{B}(\gamma)$, where $\odot$ denotes the Hadamard matrix product and $\mathbf{B}(\gamma)$ is a real-valued symmetric Toeplitz matrix, whose elements are Gaussian functions when γ is Gaussian and sinc functions when γ is uniform [10], [39]–[41].

C. Biomedical Imaging

Models (3), (5), and (7) are also relevant in biomedical imaging. In electromagnetic brain imaging [42] an array of electric and/or magnetic sensors is used to measure the electric and/or magnetic fields produced due to the electrical activity of the brain. Focal sources in the brain are modeled as equivalent current dipoles, which are parameterized by location, orientation, and strength. For a given source location and brain/sensor array geometry, the measured signal is described as the weighted sum of the contributions due to unit strength dipoles oriented in the three coordinate directions. Let $\mathbf{H}$ be an $L\times 3\,(p=3)$ matrix, whose columns are the signals at the array due to unit strength sources in the x-, y-, and z-coordinates. Then, the signal due to a source with orientation vector $\mathbf{m}$ and amplitude α may be expressed as $\mathbf{s}=\mathbf{H}\mathbf{m}\alpha$. If $\mathbf{m}$ is assumed to be known based on MRI and anatomical constraints, then $\mathbf{s}$ can be written as (3) by defining $\boldsymbol{\psi}=\mathbf{H}\mathbf{m}/\|\mathbf{H}\mathbf{m}\|_2$ and $s=\|\mathbf{H}\mathbf{m}\|_2\alpha$. If $\mathbf{m}$ is assumed to be unknown but fixed, and we decompose $\mathbf{H}$ as $\mathbf{H}=\boldsymbol{\Psi}\mathbf{F}$, where the $L\times p$ matrix $\boldsymbol{\Psi}$ is an orthonormal basis for $\langle\mathbf{H}\rangle$, then we may write $\mathbf{s}$ as in (5) by defining $\mathbf{b}_o=\mathbf{F}\mathbf{m}/\|\mathbf{F}\mathbf{m}\|_2$ and $\mathbf{s}=\|\mathbf{F}\mathbf{m}\|_2\alpha$. Finally, if $\mathbf{m}$ is assumed to be random with known covariance $\mathbf{R}_{mm}=E[\mathbf{m}\mathbf{m}^H]$, as in the rotating dipole model of [43], then the signal $\mathbf{s}$ may be modeled as in (7) by defining $\mathbf{b}=\mathbf{F}\mathbf{m}/E[\mathbf{m}^H\mathbf{F}^H\mathbf{F}\mathbf{m}]$ and $s=E[\mathbf{m}^H\mathbf{F}^H\mathbf{F}\mathbf{m}]\alpha$.

In Sections III–V, we will develop eigenvalue beamforming methods to separate signals of the form (3), (5), and (7) from interference and noise. We treat $\mathbf{s}$ as a wavefront and use the terminology of sensor array processing for convenience.

III. Multirank MVDR Beamforming

Let $y=\mathbf{w}^H\mathbf{x}$ be the output of a vector beamformer $\mathbf{w}\in\mathbb{C}^L$, applied to the array measurement vector $\mathbf{x}\in\mathbb{C}^L$. In standard MVDR beamforming we design $\mathbf{w}$ to minimize the output power $E[yy^H]=E[(\mathbf{w}^H\mathbf{x})(\mathbf{w}^H\mathbf{x})^H]$ under the constraint (u.c.) that the beamformer produces a unit-magnitude response to a waveform with a *known* signature vector $\boldsymbol{\psi}$. That is

$$\min_{\mathbf{w}} P=\mathbf{w}^H\mathbf{R}\mathbf{w}\ \text{u.c.}\ \mathbf{w}^H\boldsymbol{\psi}=q \tag{11}$$

where $\mathbf{R}=E[\mathbf{x}\mathbf{x}^H]$ is the covariance of the array measurement vector $\mathbf{x}$. The constraint $\mathbf{w}^H\boldsymbol{\psi}=q$, $|q|^2=1$, guarantees that the beamformer yields the desired response q to any wavefront with the known signature vector $\boldsymbol{\psi}$. The MVDR beamformer performs well and predictably when the signal model is of the form (3). However, when the signal of interest follows (5) or (7), the MVDR beamformer cannot match to the unknown signature vector and its performance degrades unpredictably.

For signals of the form (5) and (7), where the p-dimensional signal subspace $\langle\boldsymbol{\Psi}\rangle$ is known, but the signal orientation is unknown, it is more natural to design a *matrix beamformer* $\mathbf{W}=[\mathbf{w}_1,\ldots\mathbf{w}_r]\in\mathbb{C}^{L\times r}$ and control the beamformer response in the subspace $\langle\boldsymbol{\Psi}\rangle$, which contains the signal of interest. Hence, we constrain our matrix beamformer to satisfy

$$\mathbf{W}^H\boldsymbol{\Psi}=\mathbf{Q}^H \tag{12}$$

where $\mathbf{Q}$ is a $p\times r$ $(r\le p)$ left-orthogonal matrix, i.e., $\mathbf{Q}^H\mathbf{Q}=\mathbf{I}_{r\times r}$. This subspace constraint is equivalent to the constraint $\mathbf{W}^H\boldsymbol{\Psi}[\,\mathbf{Q}\quad\mathbf{Q}_\star\,]=[\,\mathbf{I}\quad\mathbf{0}\,]$ where $[\,\mathbf{Q}\quad\mathbf{Q}_\star\,]\in\mathbb{C}^{p\times p}$ is an orthogonal matrix. This shows that $\mathbf{W}^H$ in (12) images the r linear combinations (or vectors) $\boldsymbol{\Psi}\mathbf{Q}$ as $\mathbf{I}$ and the $p-r$ linear combinations $\boldsymbol{\Psi}\mathbf{Q}_\star$ as zero. These are called *distortionless* and *zero-forcing* constraints, respectively. The problem of choosing $\mathbf{Q}$ is deferred to Section IV. For now, we assume $\mathbf{Q}$ is an arbitrary left-orthogonal matrix.

The matrix beamformer $\mathbf{W}$ images the array measurement vector $\mathbf{x}$ to the beamformer output vector $\mathbf{y}=\mathbf{W}^H\mathbf{x}$. We wish to design $\mathbf{W}$ to minimize the output power $\mathrm{tr}\{E[\mathbf{y}\mathbf{y}^H]\}=\mathrm{tr}\{\mathbf{W}^H\mathbf{R}\mathbf{W}\}$, while forcing the subspace constraint in (12):

$$\min_{\mathbf{W}\in\mathbb{W}} P=\mathrm{tr}\{\mathbf{W}^H\mathbf{R}\mathbf{W}\}\ \text{u.c.}\ \mathbf{W}^H\boldsymbol{\Psi}=\mathbf{Q}^H. \tag{13}$$

This may be viewed as a *multirank* generalization of the standard MVDR beamformer. We note that multirank beamforming problems of the form (13) have been considered in [19] and [20]. In [19] and [20], the constraint matrix $\mathbf{Q}$ is prespecified or data independent. When $\mathbf{W}$ and $\mathbf{Q}$ are vectors, the constraint in (13) is similar in form to the constraint of a Frost beamformer [22]. Note that the desired response in the Frost beamformer is also prespecified and data independent.

The solution to (13) may be easily determined using the method of Lagrange multipliers and completing the square to obtain the optimum rank-r MVDR beamformer $\mathbf{W}=\mathbf{W}_o$ and the minimum output power $P=P_o$:

$$\mathbf{W}_o=\mathbf{R}^{-1}\boldsymbol{\Psi}(\boldsymbol{\Psi}^H\mathbf{R}^{-1}\boldsymbol{\Psi})^{-1}\mathbf{Q}, \tag{14}$$

$$\begin{aligned}P_o&=\mathrm{tr}\left\{\mathbf{W}_o^H\mathbf{R}\mathbf{W}_o\right\}\\&=\mathrm{tr}\left\{\mathbf{Q}^H(\boldsymbol{\Psi}^H\mathbf{R}^{-1}\boldsymbol{\Psi})^{-1}\mathbf{Q}\right\}.\end{aligned} \tag{15}$$

The multirank MVDR beamformer $\mathbf{W}_o^H$ may also be formulated using a generalization of the GSC introduced in [26]. Although the GSC is not necessary for implementing $\mathbf{W}_o$, it is essential for understanding and interpreting multirank MVDR beamforming. Let $\mathbf{G}\in\mathbb{C}^{L\times(L-p)}$ be a left-orthogonal matrix that makes $[\,\boldsymbol{\Psi}\quad\mathbf{G}\,]\in\mathbb{C}^{L\times L}$ unitary and express the multirank beamformer $\mathbf{W}_o$ as

$$\mathbf{W}_o=[\boldsymbol{\Psi}-\mathbf{G}\mathbf{F}]\mathbf{Q} \tag{16}$$

where $\mathbf{F}=(\mathbf{G}^H\mathbf{R}\mathbf{G})^{-1}\mathbf{G}^H\mathbf{R}\boldsymbol{\Psi}$. The beamformer output $\mathbf{y}=\mathbf{W}_o^H\mathbf{x}$ is then written as

$$\mathbf{y}=\mathbf{Q}^H[\mathbf{u}-\mathbf{F}^H\mathbf{v}]=\mathbf{Q}^H\mathbf{e}, \tag{17}$$

where $\mathbf{u}=\boldsymbol{\Psi}^H\mathbf{x}$, $\mathbf{v}=\mathbf{G}^H\mathbf{x}$, and $\mathbf{e}=\mathbf{u}-\mathbf{F}^H\mathbf{v}$ are the vectors shown in the GSC diagram in Fig. 3.

In the GSC, the vector $\mathbf{x}$ is decomposed into two sets of coordinates $\mathbf{u}=\boldsymbol{\Psi}^H\mathbf{x}$ and $\mathbf{v}=\mathbf{G}^H\mathbf{x}$, with the composite covariance matrix

$$\begin{aligned}&E\begin{bmatrix}\mathbf{u}\\\mathbf{v}\end{bmatrix}[\,\mathbf{u}^H\quad\mathbf{v}^H\,]\\&\quad=\begin{bmatrix}\left(\mathbf{R}_{uu}=\boldsymbol{\Psi}^H\mathbf{R}\boldsymbol{\Psi}\right)&\left(\mathbf{R}_{uv}=\boldsymbol{\Psi}^H\mathbf{R}\mathbf{G}\right)\\\left(\mathbf{R}_{vu}=\mathbf{G}^H\mathbf{R}\boldsymbol{\Psi}\right)&\left(\mathbf{R}_{vv}=\mathbf{G}^H\mathbf{R}\mathbf{G}\right)\end{bmatrix}.\end{aligned} \tag{18}$$

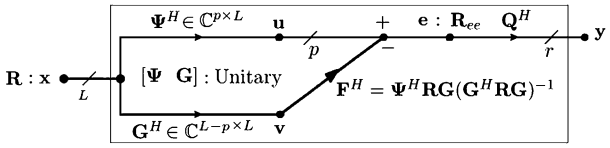

Fig. 3. Generalized sidelobe canceller.

The top branch output $\mathbf{u}$ is estimated from the bottom branch output $\mathbf{v}$, using the LMMSE filter $\mathbf{R}_{uv}\mathbf{R}_{vv}^{-1} = \mathbf{F}^H$. Hence, $\mathbf{e} = \mathbf{u} - \mathbf{F}^H\mathbf{v}$ is the error in estimating $\mathbf{u}$ from $\mathbf{v}$. The error covariance $\mathbf{R}_{ee} = E[\mathbf{e}\mathbf{e}^H]$ is given by

$$\mathbf{R}_{ee} = \mathbf{\Psi}^H\mathbf{R}\mathbf{\Psi} - \mathbf{\Psi}^H\mathbf{R}\mathbf{G}(\mathbf{G}^H\mathbf{R}\mathbf{G})^{-1}\mathbf{G}^H\mathbf{R}\mathbf{\Psi} \tag{19}$$

which may also be expressed as

$$\mathbf{R}_{ee} = (\mathbf{\Psi}^H\mathbf{R}^{-1}\mathbf{\Psi})^{-1}. \tag{20}$$

The output covariance matrix $\mathbf{R}_{yy} = E[\mathbf{y}\mathbf{y}^H]$ and the output power $P_o = \mathrm{tr}\{\mathbf{R}_{yy}\}$ of the multirank MVDR beamformer are expressed in terms of $\mathbf{R}_{ee}$ as

$$\mathbf{R}_{yy} = E[\mathbf{y}\mathbf{y}^H] = E[\mathbf{Q}^H\mathbf{e}\mathbf{e}^H\mathbf{Q}] = \mathbf{Q}^H\mathbf{R}_{ee}\mathbf{Q} \tag{21}$$

$$P_o = \mathrm{tr}\{\mathbf{R}_{yy}\} = \mathrm{tr}\left\{\mathbf{Q}^H\mathbf{R}_{ee}\mathbf{Q}\right\}. \tag{22}$$

The top branch of the GSC passes the part of $\mathbf{x}$ that lies in the signal subspace $\langle\mathbf{\Psi}\rangle$ and blocks the part of $\mathbf{x}$ that lies in the orthogonal subspace $\langle\mathbf{G}\rangle = \langle\mathbf{\Psi}\rangle^{\perp}$. Therefore, the signal $\mathbf{s}$ is passed through the top branch along with the parts of interference and noise that lie in $\langle\mathbf{\Psi}\rangle$. That is $\mathbf{u} = \mathbf{\Psi}^H\mathbf{s}$ contains the signal of interest and the resolutions of the interference and noise onto $\langle\mathbf{\Psi}\rangle$. The bottom branch of the GSC passes the parts of interference and noise that lie in $\langle\mathbf{G}\rangle$. However, due to the orthogonality of $\langle\mathbf{\Psi}\rangle$ and $\langle\mathbf{G}\rangle$ the signal does not leak through the bottom branch, and $\mathbf{v} = \mathbf{G}^H\mathbf{x}$ contains the resolutions of the interference and noise onto $\langle\mathbf{G}\rangle$, but no signal. In estimating $\mathbf{u}$ from $\mathbf{v}$, the interference that has leaked through the signal subspace $\langle\mathbf{\Psi}\rangle$ is estimated from the interference that lies in $\langle\mathbf{\Psi}\rangle^{\perp}$ and subtracted out. Thus, the error vector $\mathbf{e}$ contains the signal of interest, and reduced interference and noise. The output vector $\mathbf{y}$ is formed by transforming the error vector $\mathbf{e}$ by the constraint matrix $\mathbf{Q}^H$. This is a subspace selection or coordinate selection step, which may be designed to extract the signal of interest from $\mathbf{e}$. In beamforming applications the matrix $\mathbf{\Psi}$ may be steered to a particular angle θ, or more generally scanned to a particular value of a parameter of the uncertain signature vector, and at each θ the output power $P_o = P_o(\theta)$ is computed:

$$\begin{aligned} P_o(\theta) &= \mathrm{tr}\left\{\mathbf{Q}^H\mathbf{R}_{ee}(\theta)\mathbf{Q}\right\} \\ &= \mathrm{tr}\left\{\mathbf{Q}^H(\mathbf{\Psi}^H(\theta)\mathbf{R}^{-1}\mathbf{\Psi}(\theta))^{-1}\mathbf{Q}\right\}. \end{aligned} \tag{23}$$

The plot of the output power $P_o(\theta)$ versus θ is called a *bearing response pattern*.

Remark 2: From (9), it is easy to see that the basis $\mathbf{\Psi} = \mathbf{\Psi}(\theta)$ corresponding to a Slepian subspace steered to angle θ may be expressed as

$$\mathbf{\Psi}(\theta) = \mathbf{D}(e^{j\theta})\mathbf{\Psi}(0) \tag{24}$$

where $\mathbf{D}(e^{j\theta}) = \mathrm{diag}[1, e^{j\theta}, \ldots, e^{j(L-1)\theta}]$ corresponds to relative phasings on a ULA steered to *electrical angle* θ and $\mathbf{\Psi}(0)$ is the Slepian basis corresponding to angular bandwidth $[-\beta\pi, +\beta\pi]$, centered at $\theta = 0$. The electrical angle θ is related to the geometrical angle ϕ as $\theta = 2\pi(d/\lambda)\sin\phi$.

IV. Subspace Selection for Eigenvalue Beamforming: Matched Direction Beamforming Versus Matched Subspace Beamforming

We now address the design of the constraint matrix $\mathbf{Q}$ to resolve standing waves (signals of the form (5)) and fluctuating waves (signals of the form (7)). For ease of exposition, we assume that the interference covariance matrix $\mathbf{R}_{\nu\nu}$ is rank-1 of the form $\mathbf{R}_{\nu\nu} = \sigma_\nu^2\boldsymbol{\nu}\boldsymbol{\nu}^H$, so that $\mathbf{R} = \mathbf{R}_{ss} + \sigma_\nu^2\boldsymbol{\nu}\boldsymbol{\nu}^H + \sigma_n^2\mathbf{I}_{L\times L}$. Inserting $\mathbf{R}$ in (19), using $\mathbf{G}^H\mathbf{\Psi} = 0$ and the matrix inversion lemma [44], we obtain the error covariance matrix

$$\begin{aligned} \mathbf{R}_{ee} &= (\mathbf{\Psi}^H\mathbf{R}^{-1}\mathbf{\Psi})^{-1} \\ &= \mathbf{\Psi}^H\mathbf{R}_{ss}\mathbf{\Psi} + \sigma_\nu^2\frac{\sigma_n^2}{\sigma_n^2 + \sigma_\nu^2\boldsymbol{\nu}^H\mathbf{P}_{\mathbf{\Psi}}^{\perp}\boldsymbol{\nu}}\mathbf{\Psi}^H\boldsymbol{\nu}\boldsymbol{\nu}^H\mathbf{\Psi} + \sigma_n^2\mathbf{I}_{p\times p}. \end{aligned} \tag{25}$$

The first term in (25), $\mathbf{\Psi}^H\mathbf{R}_{ss}\mathbf{\Psi}$, is the signal covariance matrix after it is passed through the top branch of the GSC. For standing waves (5) with $\mathbf{R}_{ss}$ given by (6) this term is $\mathbf{\Psi}^H\mathbf{R}_{ss}\mathbf{\Psi} = \sigma_s^2\mathbf{b}_o\mathbf{b}_o^H$. For fluctuating waves (7) with the multirank covariance $\mathbf{R}_{ss}$ given by (8) we have $\mathbf{\Psi}^H\mathbf{R}_{ss}\mathbf{\Psi} = \sigma_s^2\mathbf{\Lambda}$, where $\mathbf{\Lambda} = \mathrm{diag}(\lambda_1, \ldots, \lambda_p)$ is diagonal.[2] The second term on the right-hand side (RHS) of (25) is the covariance matrix for the interfering wavefront, after it is suppressed by the GSC. The top branch of the GSC reduces the interference power σ_ν^2 by a factor of $||\mathbf{\Psi}^H\boldsymbol{\nu}||^2$. The bottom branch further suppresses the interference power by a factor of $\eta^2 = \sigma_n^2/\left(\sigma_n^2 + \sigma_\nu^2\boldsymbol{\nu}^H\mathbf{P}_{\mathbf{\Psi}}^{\perp}\boldsymbol{\nu}\right) < 1$.

Remark 3: If the bottom branch of the GSC is switched off, the beamformer $\mathbf{W}_o$ becomes a multirank Bartlett beamformer [36], [37], and $\mathbf{R}_{ee}$ will reduce to $\mathbf{R}_{uu}$:

$$\begin{aligned} \mathbf{R}_{uu} &= \mathbf{\Psi}^H\mathbf{R}\mathbf{\Psi} \\ &= \mathbf{\Psi}^H\mathbf{R}_{ss}\mathbf{\Psi} + \sigma_\nu^2\mathbf{\Psi}^H\boldsymbol{\nu}\boldsymbol{\nu}^H\mathbf{\Psi} + \sigma_n^2\mathbf{I}_{p\times p}. \end{aligned} \tag{26}$$

Thus, the factor η^2 represents the extra interference suppression obtained with a multirank MVDR beamformer compared to a multirank Bartlett beamformer.

The output power of the multirank MVDR beamformer $\mathbf{W}_o^H$ is related to the error covariance matrix $\mathbf{R}_{ee}$ via (22). We now consider choosing $\mathbf{Q}$ so that $\mathrm{tr}\left\{\mathbf{Q}^H\mathbf{R}_{ee}\mathbf{Q}\right\}$ captures the signal power for standing waves and for fluctuating waves.

A. Standing Waves and Matched Direction Beamforming

In the case of standing waves (5), the error covariance matrix $\mathbf{R}_{ee}$ is given by

$$\mathbf{R}_{ee} = \sigma_s^2\mathbf{b}_o\mathbf{b}_o^H + \sigma_\nu^2\frac{\sigma_n^2}{\sigma_n^2 + \sigma_\nu^2\boldsymbol{\nu}^H\mathbf{P}_{\mathbf{\Psi}}^{\perp}\boldsymbol{\nu}}\mathbf{\Psi}^H\boldsymbol{\nu}\boldsymbol{\nu}^H\mathbf{\Psi} + \sigma_n^2\mathbf{I}_{p\times p}. \tag{27}$$

[2]Without loss of generality, we assume $\mathbf{R}_{bb} = \mathbf{\Lambda} = \mathrm{diag}(\lambda_1, \ldots, \lambda_p)$, since the known $\mathbf{R}_{bb}$ can always be diagonalized and the eigenvector matrix of $\mathbf{R}_{bb}$ can be absorbed in $\mathbf{\Psi}$.

If the signal subspace $\langle \mathbf{\Psi} \rangle$ and the interference subspace $\langle \boldsymbol{\nu} \rangle$ are well separated, then the interference will be suppressed by the GSC through $\mathbf{\Psi}^H$ and η^2. In that case, the rank-1 signal term $\sigma_s^2 \mathbf{b}_0 \mathbf{b}_0^H$ contributes to only the largest eigenvalue of $\mathbf{R}_{ee}$. Therefore, $\mathbf{Q}$ must carry the dominant eigenvector of $\mathbf{R}_{ee}$. The dominant eigenvector of $\mathbf{R}_{ee}$ identifies $\mathbf{b}_0$ and the dominant eigenvalue of $\mathbf{R}_{ee}$ gives a noisy but interference free estimate of σ_s^2.

However, if the interference term $\sigma_\nu^2 \eta^2 \mathbf{\Psi}^H \boldsymbol{\nu}\boldsymbol{\nu}^H \mathbf{\Psi}$ is significant, the signal and interference terms together will determine the two largest eigenvalues of $\mathbf{R}_{ee}$. Thus, to prevent loss of signal power, $\mathbf{Q}$ must select the two most dominant eigenvectors of $\mathbf{R}_{ee}$. The sum of the two largest eigenvalues of $\mathbf{R}_{ee}$ then captures all of the signal power, plus a fraction of the interference power and the noise power. In the more general case where the interference covariance matrix is not negligible and has rank $r-1$ ($r \leq p$), or $r-1$ non-negligible interferer are present, the matrix $\mathbf{Q}$ must select the r dominant eigenvectors of $\mathbf{R}_{ee}$ to avoid loss of signal power. The sum of the r largest eigenvalues of $\mathbf{R}_{ee}$ captures all of the signal power, and we may estimate the signal power at the multirank beamformer output as

$$\hat{\sigma}_s^2 = \mathrm{tr}\{\mathbf{Q}^H \mathbf{R}_{ee} \mathbf{Q}\} = \sum_{i=1}^{r} ev_i(\mathbf{R}_{ee}). \tag{28}$$

Each eigenvalue of $\mathbf{R}_{ee}$ captures an unknown fraction of the signal plus interference power, plus σ_n^2.

The multirank beamformer $\mathbf{W}_o$, constructed using the dominant eigenvectors of $\mathbf{R}_{ee}$, may be called a *matched direction beamformer*, as it is designed to resolve signals that are drawn from an unknown direction $\langle \mathbf{\Psi} \mathbf{b}_o \rangle$ inside the known subspace $\langle \mathbf{\Psi} \rangle$.

Remark 4: Matched direction beamforming may be posed as a constrained max-min problem of the form

$$\max_{\mathbf{Q} \in \overline{\mathbb{Q}}} \left\{ \min_{\mathbf{W} \in \mathbb{W}} P = \mathrm{tr}\{\mathbf{W}^H \mathbf{R} \mathbf{W}\} \text{ u.c. } \mathbf{W}^H \mathbf{\Psi} = \mathbf{Q}^H \right\} \tag{29}$$

where $\mathbb{Q}$ is the set of all $p \times r$ left-orthogonal matrices. Thus, our matched direction beamformers generalize the minimum variance CDMA receivers of [23], [24] and the biomagnetic spatial filters of [25], both of which are vector beamformers $\mathbf{w} \in \mathbb{C}^L$ that solve the max-min problem

$$\max_{\mathbf{q} \in \overline{\mathbb{Q}}} \left\{ \min_{\mathbf{w}} P = \mathrm{tr}\{\mathbf{w}^H \mathbf{R} \mathbf{w}\} \text{ u.c. } \mathbf{w}^H \mathbf{\Psi} \mathbf{q} = 1 \right\} \tag{30}$$

where $\overline{\mathbb{Q}}$ is the set of all $p \times 1$ unit-norm complex vectors.

B. Fluctuating Waves and Matched Subspace Beamforming

We now consider the case of fluctuating waves (7), where the signal covariance $\mathbf{R}_{ss}$ is $\mathbf{R}_{ss} = \sigma_s^2 \mathbf{\Psi}^H \mathbf{\Lambda} \mathbf{\Psi}$. For exposition we consider the Slepian case where $\mathbf{\Lambda} = (1/p)\mathbf{I}$. So the error covariance matrix $\mathbf{R}_{ee}$ in (25) is given by

$$\mathbf{R}_{ee} = \frac{\sigma_s^2}{p} \mathbf{I}_{p \times p} + \sigma_\nu^2 \eta^2 \mathbf{\Psi}^H \boldsymbol{\nu}\boldsymbol{\nu}^H \mathbf{\Psi} + \sigma_n^2 \mathbf{I}_{p \times p}. \tag{31}$$

When the interference term $\sigma_\nu^2 \eta^2 \mathbf{\Psi}^H \boldsymbol{\nu}\boldsymbol{\nu}^H \mathbf{\Psi}$ is negligible, all the eigenvalues of $\mathbf{R}_{ee}$ are equal to $\mathrm{ev}_i(\mathbf{R}_{ee}) = \sigma_s^2/p + \sigma_n^2$, $i = 1, \ldots, p$. Hence, $\mathbf{Q}$ may be selected as any collection of $r \leq p$ of the eigenvectors of $\mathbf{R}_{ee}$ and σ_s^2 may be estimated as $\hat{\sigma}_s^2 = \mathrm{tr}\{\mathbf{Q}^H \mathbf{R}_{ee} \mathbf{Q}\} = (r/p)\sigma_s^2 + r\sigma_n^2$. When the interference term is significant, the largest eigenvalue of $\mathbf{R}_{ee}$ is contaminated by the interference. However, the remaining eigenvalues are equal to $\mathrm{ev}_i(\mathbf{R}_{ee}) = \sigma_s^2/p + \sigma_n^2, i = 2, \ldots, p$. Thus, interference is eliminated if $\mathbf{Q}$ is selected from the $r < p$ subdominant eigenvectors of $\mathbf{R}_{ee}$. In this case an estimate of the signal power at the beamformer output is

$$\hat{\sigma}_s^2 = \mathrm{tr}\left\{\mathbf{Q}^H \mathbf{R}_{ee} \mathbf{Q}\right\} = \sum_{i=p}^{p-r_s+1} ev_i(\mathbf{R}_{ee}). \tag{32}$$

We have deliberately written the index of the summation in (32) from p to $p - r_s + 1$ to emphasize that we start by including the most subdominant eigenvector of $\mathbf{R}_{ee}$ in $\mathbf{Q}$ and work toward more dominant eigenvectors. In Section IV-C, we show that the most subdominant eigenvalue of $\mathbf{R}_{ee}$ gives the best angular resolution for resolving fluctuating waves, and that there exists a tradeoff between angular resolution and the fraction of signal power captured at the beamformer output.

The beamformer $\mathbf{W}_o$, constructed from the subdominant eigenvectors of $\mathbf{R}_{ee}$, resolves signals that are drawn from a known multidimensional subspace, and is termed a *matched subspace beamformer*. Provided that the rank of the interference term in $\mathbf{R}_{ee}$ is less than p, the matched subspace beamformer $\mathbf{W}_o$ yields a noisy but interference free estimate of σ_s^2. Since each eigenvalue of $\mathbf{R}_{ee}$ captures $1/p$ of the signal power σ_s^2, we could normalize (32) by p/r to make the signal term in $\hat{\sigma}_s^2$ equal to σ_s^2. However, this would scale the noise power by a factor of p/r.

When the known $\mathbf{\Lambda} = \mathrm{diag}[\lambda_1, \ldots, \lambda_p]$ is not proportional to the identity matrix, then $\mathbf{R}_{ee} = (\sigma_s^2/p)\mathbf{\Lambda} + \sigma_\nu^2 \eta^2 \mathbf{\Psi}^H \boldsymbol{\nu}\boldsymbol{\nu}^H \mathbf{\Psi} + \sigma_n^2 \mathbf{I}_{p \times p}$. If the signal and interference subspaces are well separated the interference will be suppressed and the ith eigenvalue of $\mathbf{R}_{ee}$ will capture $\lambda_i \sigma_s^2$ of the signal power, and an estimate of the signal power at the beamformer output is given by (32). Since $\lambda_1 \geq \cdots \geq \lambda_p > 0$, the most subdominant eigenvalue of $\mathbf{R}_{ee}$ captures the smallest fraction $\lambda_p \sigma_s^2$ of the signal power. However, this eigenvalue gives the best angular resolution for resolving fluctuating waves. Note that normalization of $\hat{\sigma}_s^2$ by $1/(\lambda_p + \cdots + \lambda_{p-i+1})$ forces the signal power in $\hat{\sigma}_s^2$ to be σ_s^2, but scales the noise power proportionally. When the interference term is significant, but has rank $r - 1 \leq p - 1$, then the subdominant eigenvalues of $\mathbf{R}_{ee}$ provide interference free estimates of fractions of the signal power.

Remark 5: Matched subspace beamforming may be posed as a min-min problem of the form

$$\min_{\mathbf{Q} \in \mathbb{Q}} \left\{ \min_{\mathbf{W} \in \mathbb{W}} P = \mathrm{tr}\{\mathbf{W}^H \mathbf{R} \mathbf{W}\} \text{ u.c. } \mathbf{W}^H \mathbf{\Psi} = \mathbf{Q}^H \right\} \tag{33}$$

where $\mathbb{Q}$ is the set of all $p \times r$ left orthogonal matrices. The min-min problem in (33) is equivalent to minimizing the output power $P = \mathrm{tr}\{\mathbf{W}^H \mathbf{R} \mathbf{W}\}$ under the quadratic constraint $\mathbf{W}^H \mathbf{\Psi} \mathbf{\Psi}^H \mathbf{W} = \mathbf{I}$ [45]. This establishes a connection between matched subspace beamformers and robust adaptive beamformers of [10], which enforce a quadratic constraint of the form $\mathbf{w}^H \mathbf{R}_{ss} \mathbf{w} = 1$.

C. Eigenvalue Beamforming

In both matched direction and matched subspace beamforming, the ith column of the multirank beamformer $\mathbf{W}_o = [\mathbf{w}_{o,1}, \ldots, \mathbf{w}_{o,r}]$ is an *eigenvalue beamformer* of the form

$$\mathbf{w}_{o,i} = \mathbf{R}^{-1}\Psi\left(\Psi^H\mathbf{R}^{-1}\Psi\right)^{-1}\mathbf{q}_i \tag{34}$$

where $\mathbf{q}_i$ is the ith column of $\mathbf{Q} = [\mathbf{q}_1, \ldots, \mathbf{q}_r]$. The output power of $\mathbf{w}_{o,i}$, given by $P_{o,i} = \mathbf{w}_{o,i}^H\mathbf{R}\mathbf{w}_{o,i} = \mathbf{q}_i^H\mathbf{R}_{ee}\mathbf{q}_i$, is an eigenvalue of $\mathbf{R}_{ee} = (\Psi^H\mathbf{R}^{-1}\Psi)^{-1}$. In matched direction beamforming $\mathbf{q}_i$ is the ith most dominant eigenvector of $\mathbf{R}_{ee}$ and $P_{o,i}$ is the ith most dominant eigenvalue. In matched subspace beamforming $\mathbf{q}_i$ is the ith most subdominant eigenvector of $\mathbf{R}_{ee}$ and $P_{o,i}$ is its ith most subdominant eigenvalue. The eigenvalue beamformer $\mathbf{w}_{o,i}$ extracts a fraction of the signal power from an eigenmode of $\mathbf{R}_{ee}$. When we steer $\Psi(\theta)$ around in θ the eigenvalue beamformers $\mathbf{w}_{o,i}$ and their output powers vary with θ, by the virtue of their dependence on $\Psi(\theta)$. We call the plot of $P_{o,i}(\theta)$ versus θ an *eigenvalue bearing response pattern*.

Matched direction and matched subspace beamforming are diversity combining techniques, in which per mode (per subspace dimension) output powers extracted by eigenvalue beamformers are summed up to produce an estimate of the signal power. This is analogous to wireless communications where uncorrelated paths are diversity combined. When the signal power is distributed among multiple directions in the signal subspace $\langle\Psi\rangle$, either because the signal covariance is multirank or because a signal with rank-1 covariance is in the presence of interference, each eigenvalue beamformer captures a fraction of the signal power, and the sum of the output powers is a diversity combination designed to capture all of the signal power. However, we shall show next that angular resolution decreases as the fraction of the signal power captured by the multirank beamformer increases.

Each eigenvalue beamformer extracts signal information from an orthogonal subspace mode, at a different resolution. Hence, eigenvalue beamformers are fundamental for resolving signals that are drawn from a multidimensional subspace, and monitoring the output powers of eigenvalue beamformers individually can be more insightful for resolving standing and fluctuating waves than monitoring their diversity sums.

D. Resolution Analysis

In the following resolution analysis, without loss of generality, we assume that the signal subspace $\bar{\Psi} = \bar{\Psi}(\theta)$ is a Slepian subspace of dimension $p = \beta L$, which is steered around in θ. However, the argument easily extends to other signal subspaces, which in general are steered around in a parameter.

We first consider the matched subspace case. Suppose a fluctuating wave with angular bandwidth $2\beta L$, centered at $\theta = \theta_o$, and with covariance matrix $\mathbf{R}_{ss}(\theta_o) = \left(\sigma_s^2/p\right)\Psi(\theta_o)\Psi^H(\theta_o)$, is incident on the array. If the interference is negligible, then

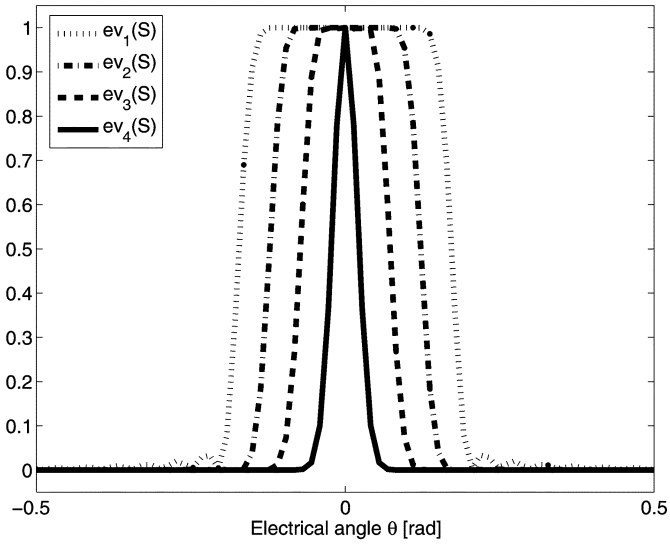

Fig. 4. Plots of the eigenvalues of $\mathbf{S}(\theta, 0)$ versus θ.

when $\Psi(\theta)$ is steered to angle θ, the error covariance matrix $\mathbf{R}_{ee}(\theta)$ is given by

$$\begin{aligned}\mathbf{R}_{ee}(\theta) &= (\Psi^H(\theta)\mathbf{R}^{-1}(\theta_o)\Psi(\theta))^{-1} \\ &= \frac{\sigma_s^2}{p}\mathbf{S}(\theta,\theta_o) + \sigma_n^2\mathbf{I}_{p\times p}\end{aligned} \tag{35}$$

where $\mathbf{S}(\theta,\theta_o) = \Psi(\theta)^H\Psi(\theta_o)\Psi(\theta_o)^H\Psi(\theta)$. The ith eigenvalue of $\mathbf{R}_{ee}(\theta)$ is equal to $\left(\sigma_s^2/p\right)\mathrm{ev}_i(\mathbf{S}(\theta,\theta_o)) + \sigma_n^2$, and it depends on the location of the source θ_o and the electrical angle θ. The eigenvalues of $\mathbf{S}(\theta,\theta_o)$ are squares of the cosines of the principal angles [46] between $\langle\Psi(\theta)\rangle$ and $\langle\Psi(\theta_o)\rangle$. When θ is far from θ_o such that the angular bandwidth $\Theta = [\theta-\beta\pi, \theta+\beta\pi]$ for $\langle\Psi(\theta)\rangle$ and $\Theta_o = [\theta_o - \beta\pi, \theta_o + \beta\pi]$ for $\langle\Psi(\theta_o)\rangle$ do not overlap, all the principal cosines between $\langle\Psi(\theta)\rangle$ and $\langle\Psi(\theta_o)\rangle$ are zero. As θ moves closer to θ_o, so that Θ and Θ_o begin to overlap, a few of the principal cosines (cosines of principal angles) become nonzero, while the rest stay close to zero. As the overlap between Θ and Θ_o increases, the number of nonzero principal cosines grows. Finally when Θ and Θ_o overlap completely all principal cosines become one. This indicates that the angular bandwidth over which $\mathbf{S}(\theta,\theta_o)$ has only one nonzero eigenvalue is wider than the angular bandwidth over which it has $p = \beta L$ nonzero eigenvalues.

Fig. 4 shows the evolution of the eigenvalues of $\mathbf{S}(\theta, 0)$ versus θ for the case where $\langle\Psi(0)\rangle$ is a $\beta L = 4$ dimensional Slepian subspace, centered at $\theta_o = 0$. We notice that as we move from the dominant eigenvalue $\mathrm{ev}_1(\mathbf{S}(\theta,\theta_o))$ towards the subdominant one $\mathrm{ev}_4(\mathbf{S}(\theta,\theta_o))$ the eigenvalue bearing response patterns around $\theta_o = 0$ become sharper. This shows that the subdominant eigenvalues of $\mathbf{R}_{ee}(\theta)$ offer higher angular resolution for resolving fluctuating waves than the dominant ones, and points to a tradeoff between angular resolution and the fraction of the signal power captured by the matched subspace beamformer. The eigenvalue beamformer associated with the most subdominant eigenvalue of $\mathbf{R}_{ee}$ provides the highest resolution, but captures only a small fraction of the signal power. We can cap-

ture a larger fraction of the signal power by diversity combining the eigenvalue beamformers associated with other subdominant eigenvalues of $\mathbf{R}_{ee}$ at the cost of reduced resolution. We present numerical examples to demonstrate this tradeoff in Section V.

Remark 6: The tradeoff between resolution and the fraction of signal power captured by the matched subspace beamformer extends to the case where $\mathbf{R}_{bb} = \mathbf{\Lambda} = [\lambda_1, \ldots, \lambda_p]$, $\lambda_1 \geq \cdots \geq \lambda_p > 0$ is diagonal, as shown in the Appendix. The most subdominant eigenvalue beamformer, which offers the highest angular resolution, captures the smallest per mode signal power $\lambda_p \sigma_s^2$.

The tradeoff between resolution and signal power also applies in the matched direction case. If the interference is negligible the most dominant eigenvalue beamformer captures all of the signal power and fixes the angular resolution. If a strong interferer is present at a nearby angle, then when $\mathbf{\Psi}(\theta)$ is steered nearby, a fraction of the signal plus interference power will be captured by the second most dominant eigenvalue of $\mathbf{R}_{ee}$. Diversity combining the two most dominant eigenvalue beamformers captures all the signal power, but allows for more leakage of power from the interferer and degrades the resolution of the source and interference.

E. Comparison With Multirank Bartlett Beamformer

If the bottom branch of the GSC is switched off, the beamformer $\mathbf{W}_o$ will reduce to a multirank Bartlett beamformer of the form $\mathbf{W}_o = \mathbf{\Psi Q}$, and the beamformer output covariance will be $\mathbf{R}_{yy} = \mathbf{Q}^H \mathbf{R}_{uu} \mathbf{Q} = \mathbf{Q}^H (\mathbf{\Psi}^H \mathbf{R} \mathbf{\Psi}) \mathbf{Q}$. We can select $\mathbf{Q}$ to retain either the dominant eigenvalues of $\mathbf{R}_{uu} = \mathbf{\Psi}^H \mathbf{R} \mathbf{\Psi}$ for *matched direction Bartlett beamforming* or the subdominant eigenvalues of $\mathbf{R}_{uu}$ for *matched subspace Bartlett beamforming*. However, we note that $\mathbf{Q}$ in this case is different than $\mathbf{Q}$ for matched direction MVDR and matched subspace MVDR beamforming, because in general the eigenvectors of $\mathbf{R}_{uu} = \mathbf{\Psi}^H \mathbf{R} \mathbf{\Psi}$ and $\mathbf{R}_{ee} = (\mathbf{\Psi}^H \mathbf{R}^{-1} \mathbf{\Psi})^{-1}$ are different. They are the same only when there is no interference. Matched direction and matched subspace MVDR beamformers always provide better interference suppression than their Bartlett counterparts, due to the extra interference reduction by η^2.

The second matrix on the RHS of (19) is positive semidefinite (PSD), so the Bartlett matrix $\mathbf{R}_{uu}(\theta) = \mathbf{\Psi}^H(\theta) \mathbf{R} \mathbf{\Psi}(\theta)$ and the error covariance matrix $\mathbf{R}_{ee}(\theta) = (\mathbf{\Psi}^H(\theta) \mathbf{R}^{-1} \mathbf{\Psi}(\theta))^{-1}$ satisfy the inequality

$$\mathbf{R}_{uu}(\theta) = \mathbf{\Psi}^H(\theta) \mathbf{R} \mathbf{\Psi}(\theta) \succeq \mathbf{R}_{ee}(\theta) = (\mathbf{\Psi}^H(\theta) \mathbf{R}^{-1} \mathbf{\Psi}(\theta))^{-1} \tag{36}$$

where $\mathbf{A} \succeq \mathbf{B}$ means that $\mathbf{A} - \mathbf{B}$ is PSD. This matrix inequality holds at every electrical angle and is true even when there is no interference.[3] The matrix inequality in (36) implies that at any given θ the ith eigenvalue of $\mathbf{R}_{uu}(\theta)$ is always greater than or equal to the ith eigenvalue of $\mathbf{R}_{ee}(\theta)$. Thus, the bearing response pattern of the ith Bartlett eigenvalue beamformer always lies on or above the bearing response pattern for the ith MVDR eigenvalue beamformer. Since both $\mathrm{ev}_i(\mathbf{R}_{uu}(\theta))$ and $\mathrm{ev}_i(\mathbf{R}_{ee}(\theta))$ capture the same amount of noise power, and peak around the same angle with nearly (within the factor η^2) the same peak value, we conclude that the ith MVDR eigenvalue beamformer has a better angular resolution than the ith Bartlett eigenvalue beamformer. Numerical examples to be presented validate this observation.

[3]Equality holds, if there is no interference and $\mathbf{\Psi}(\theta)$ is steered to the electrical angle where the signal is located.

V. Numerical Examples

We now demonstrate the role of the eigenvalue beamformers in resolving signals of the form (5) and (7), and study their performance in the presence of signal subspace mismatch using simple numerical examples. We consider a ULA with $L = 128$ elements and half-wavelength inter-element spacing $d = \lambda/2$. Four narrowband sources of the rank-1 form (5) and four sources of the rank-p form (7) are incident on the array. All sources are drawn from the $p = \beta L = 4$ dimensional Slepian subspace, so $\langle \mathbf{\Psi} \rangle$ is the four-dimensional Slepian subspace with fractional wavenumber bandwidth $\beta = 4/L$. Note that although we discussed the Slepian subspaces in the context of fluctuating waves, they are also relevant for modeling standing waves. An example is the case where the unknown orientation vector $\mathbf{b}_o$ is drawn from a distribution with known covariance, but then stays unchanged over a sequence of snapshots. The total signal power σ_s^2 for each source is $\sigma_s^2 = 1$ and the noise power σ_n^2 at each sensor element is $\sigma_n^2 = 0.1$, resulting in an input SNR of 10 dB. The four rank-1 sources are centered at electrical angles 0, 1, 2.22, and 2.29 rad, and the four rank-4 sources are centered at electrical angles -2.2, -1.3, -1, and -0.049 rad. Going from negative to positive electrical angles, the subspace orientation vectors $\mathbf{b}_o$ for the rank-1 sources are, respectively, $\mathbf{b}_o = [-0.5058, -0.6902, -0.5126, 0.0703]^T$, $\mathbf{b}_o = [0.2204, -0.2322, 0.6492, -0.6900]^T$, $\mathbf{b}_o = [0.1524, 0.0871, 0.3883, -0.9046]^T$, and $\mathbf{b}_o = [0.6006, -0.6100, -0.0347, -0.5158]^T$. These orientation vectors are fixed, but they are unknown to the beamformer. The orientation vectors for the multirank sources are randomly drawn from a distribution with covariance $\mathbf{\Lambda} = (1/p)\mathbf{I}$.

A. Known Data Covariance

In the first example, we assume that the theoretical data covariance $\mathbf{R}$ is known, and that there is no mismatch between the signal subspace $\langle \mathbf{\Psi}(\theta) \rangle$ used in beamforming and the actual signal subspace. Fig. 5(a) and (b) shows the bearing response patterns for the conventional and standard MVDR beamformers, respectively. These plots are obtained by steering the $L \times 1$ bearing vector $\boldsymbol{\psi}(\theta)$ in electrical angle θ and computing the output power $P = \boldsymbol{\psi}(\theta)^H \mathbf{R} \boldsymbol{\psi}(\theta)$ (for conventional) and $P = (\boldsymbol{\psi}(\theta)^H \mathbf{R}^{-1} \boldsymbol{\psi}(\theta))^{-1}$ (for MVDR) at each θ. As the plots show, the conventional beamformer produces false peaks near rank-1 sources and the MVDR beamformer does not resolve these sources at all. They also render wide peaks around the multirank sources and underestimate their powers by approximately 6 dB.

The behavior of the Bartlett beamformer may be explained as follows. Suppose there is no interference. Then, the power at the output of the Bartlett beamformer is $P = \boldsymbol{\psi}^H(\theta) \mathbf{R}_{ss}(\theta_o) \boldsymbol{\psi}(\theta) + \sigma_n^2$. When we sweep over θ, for a rank-1 source with covariance $\mathbf{R}_{ss}(\theta_o) = \sigma_s^2 \mathbf{\Psi}(\theta_o) \mathbf{b}_o \mathbf{b}_o^H \mathbf{\Psi}(\theta_o)^H$, there exists a narrow

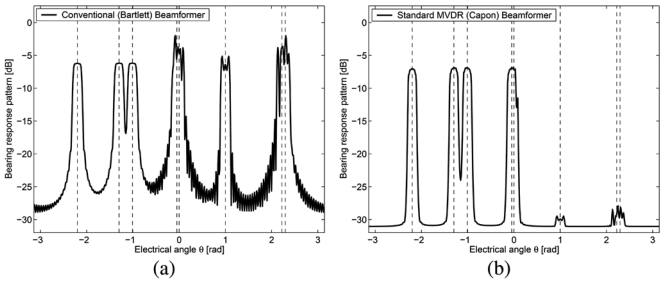

Fig. 5. Bearing response patterns for (a) conventional (Bartlett) beamformer and (b) standard MVDR beamformer. Dashed vertical lines indicate true source locations. Going from negative to positive electrical angles in each plot the first four sources generate fluctuating waves with rank-4 covariances and the next four sources generate standing waves with rank-1 covariances.

band of angles around θ_o inside which $||\boldsymbol{\psi}(\theta)^H \boldsymbol{\Psi}(\theta_o)\mathbf{b}_o||^2$ is not small. In this angular band the conventional beamformer passes a fraction of the source power and the bearing response pattern peaks. This also happens for the multirank sources with covariance $\mathbf{R}_{ss} = \left(\sigma_s^2/p\right)\boldsymbol{\Psi}(\theta_o)\boldsymbol{\Psi}^H(\theta_o)$. The power of the source in this case is equally distributed among four dimensions in the Slepian subspace and when θ is close to θ_o, $||\boldsymbol{\psi}^H(\theta)\boldsymbol{\Psi}(\theta_o)||^2$ is approximately one, and the power at the output of the beamformer is approximately $\sigma_s^2/4 = -6$ dB.

The behavior of the MVDR beamformer may be explained using the GSC in Fig. 3 by replacing $\boldsymbol{\Psi}$ with $\boldsymbol{\psi} = \boldsymbol{\psi}(\theta)$ and choosing $\mathbf{G} = \mathbf{G}(\theta)$ such that $[\boldsymbol{\psi}(\theta) \quad \mathbf{G}(\theta)]$ is unitary. The top branch of the GSC is a conventional beamformer. When θ is close to θ_o this branch passes some of the signal. This is true for both rank-1 and multirank sources. However, since $\boldsymbol{\psi}$ is mismatched with the actual signal subspace some of the signal leaks through the bottom branch, which after LMMSE estimation results in signal suppression

Fig. 6(a)–(d) shows the eigenvalue bearing response patterns $\mathrm{ev}_i(\mathbf{R}_{ee}(\theta))$, $i = 1, \ldots, 4$. We notice that the most dominant eigenvalue $\mathrm{ev}_1(\mathbf{R}_{ee})$ resolves the rank-1 sources. It captures all the power of the rank-1 sources at $\theta = 0$ and $\theta = 1$ rad. It also captures a large fraction of the powers of the rank-1 sources at $\theta = 2.22$ and $\theta = 2.29$ rad. However, since each source acts as an interference for the other a small fraction (-18 dB) of the signal power is captured by the second most dominant eigenvalue $\mathrm{ev}_2(\mathbf{R}_{ee})$. The subdominant eigenvalues $\mathrm{ev}_3(\mathbf{R}_{ee})$ and $\mathrm{ev}_4(\mathbf{R}_{ee})$ in Fig. 6(c) and (d) show no indication of presence of the rank-1 sources.

The dominant eigenvalue $\mathrm{ev}_1(\mathbf{R}_{ee})$ also gives interference free, but noisy, estimates of a fraction of the power of the multirank sources, as the interference nearby is sufficiently suppressed by the GSC. The peak values of $\mathrm{ev}_1(\mathbf{R}_{ee}(\theta))$ at locations of multirank sources are approximately $\sigma_s^2/p + \sigma_n^2 = -6$ dB, which is consistent with the signal covariance model $\mathbf{R}_{ss} = \left(\sigma_s^2/p\right)\boldsymbol{\Psi}\boldsymbol{\Psi}^H$. However, note that $\mathrm{ev}_1(\mathbf{R}_{ee}(\theta)$ is wider around multirank sources than the subdominant eigenvalue bearing response patterns $\mathrm{ev}_i(\mathbf{R}_{ee}(\theta))$, $i = 2, 3, 4$, and thus offers worse angular resolution. In particular the multirank sources at $\theta = -1.3$ and $\theta = -1$ are not well-resolved by $\mathrm{ev}_1(\mathbf{R}_{ee}(\theta))$.

Fig. 6(b)–(d) shows that each of the subdominant eigenvalues $\mathrm{ev}_2(\mathbf{R}_{ee})$, $\mathrm{ev}_3(\mathbf{R}_{ee})$, $\mathrm{ev}_4(\mathbf{R}_{ee})$ captures a fraction ($\sigma_s^2/4$ in this example) of the power of the multirank sources. They also show that the most subdominant eigenvalue $\mathrm{ev}_4(\mathbf{R}_{ee})$ offers the highest angular resolution for resolving multirank sources. We can diversity combine the eigenvalue beamformers (multirank matched direction and matched subspace beamforming) to capture a larger fraction of the signal power at the expense of resolution.

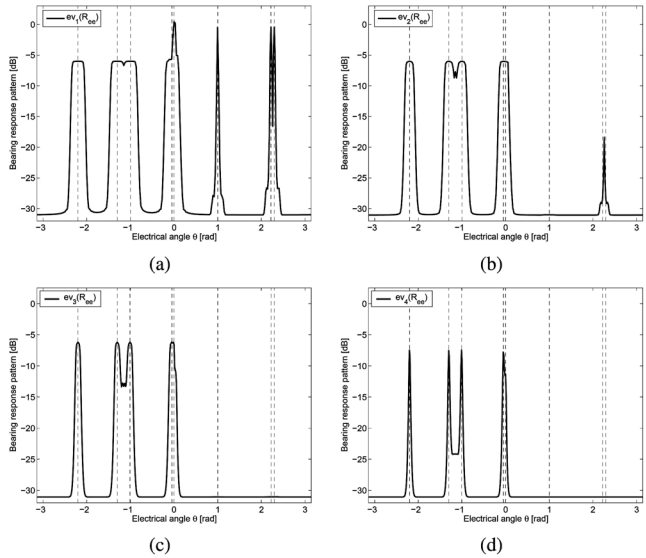

Fig. 6. MVDR Eigenvalue bearing response patterns: (a) $\mathrm{ev}_1(\mathbf{R}_{ee}(\theta))$, (b) $\mathrm{ev}_2(\mathbf{R}_{ee}(\theta))$, (c) $\mathrm{ev}_3(\mathbf{R}_{ee}(\theta))$, and (d) $\mathrm{ev}_4(\mathbf{R}_{ee}(\theta))$. Dashed vertical lines indicate true source locations. Going from negative to positive electrical angles in each plot the first four sources generate fluctuating waves with rank-4 covariances and the next four sources generate standing waves with rank-1 covariances.

Fig. 7(a)–(d) shows the Bartlett eigenvalue bearing response patterns $\mathrm{ev}_i(\mathbf{R}_{uu}(\theta))$, $i = 1, \ldots, 4$. Each of the subdominant eigenvalues of $\mathbf{R}_{uu}(\theta)$ captures the same fraction of the signal power as its MVDR counterpart. However, the most dominant Bartlett eigenvalue beamformer no longer provides an interference free estimate of the power of the multirank source at $\theta = -0.049$ rad, as it can not sufficiently suppress the rank-1 interferer at $\theta = 0$ rad. Furthermore, the resolution of each Bartlett eigenvalue beamformer around a multirank source is less than the resolution of its MVDR counterpart. For example, while the most dominant Bartlett eigenvalue beamformer resolves the rank-1 signals at $\theta = 0$ and $\theta = 1$ rad it fails to resolve the two rank-1 sources at $\theta = 2.22$ and $\theta = 2.29$ rad, which are close in angle. Comparison of $\mathrm{ev}_1(\mathbf{R}_{uu}(\theta))$ and $\mathrm{ev}_2(\mathbf{R}_{uu}(\theta))$ with $\mathrm{ev}_1(\mathbf{R}_{ee}(\theta))$ and $\mathrm{ev}_2(\mathbf{R}_{ee}(\theta))$ around the rank-1 sources at $\theta = 2.22$ and $\theta = 2.29$ rad clearly shows the superior interference suppression capability of MVDR eigenvalue beamformers.

B. Experimental Data Covariance

In most applications the data covariance matrix $\mathbf{R}$ is not known and has to be estimated from multiple array snapshots. Assuming N copies of the array measurement vector $\mathbf{x}$, say $\mathbf{x}[1], \ldots, \mathbf{x}[N]$, are available, we may use the sample covariance matrix $\hat{\mathbf{R}} = (1/N)\sum_{n=1}^{N} \mathbf{x}[n]\mathbf{x}[n]^H$ in place of $\mathbf{R}$. We consider the case where the number of data samples N is $N = 1.5L = 192$. The type of sources and their locations

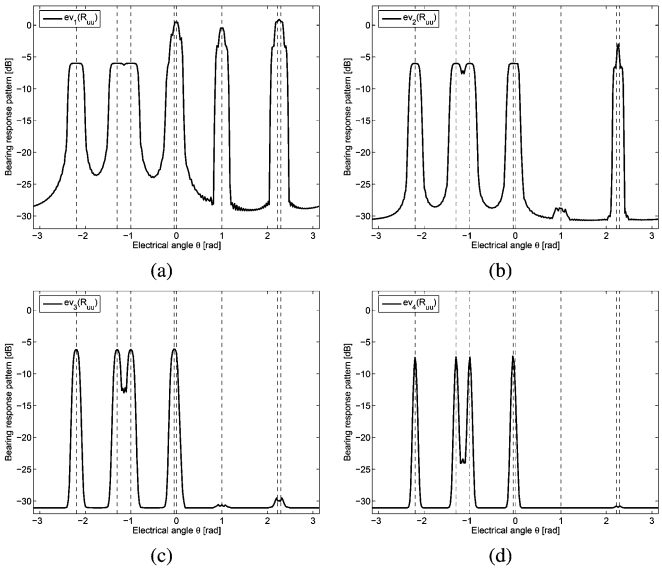

Fig. 7. Bartlett eigenvalue bearing response patterns: (a) $\mathrm{ev}_1(\mathbf{R}_{uu}(\theta))$, (b) $\mathrm{ev}_2(\mathbf{R}_{uu}(\theta))$, (c) $\mathrm{ev}_3(\mathbf{R}_{uu}(\theta))$, and (d) $\mathrm{ev}_4(\mathbf{R}_{uu}(\theta))$. Dashed vertical lines indicate true source locations. Going from negative to positive electrical angles in each plot the first four sources generate fluctuating waves with rank-4 covariances and the next four sources generate standing waves with rank-1 covariances.

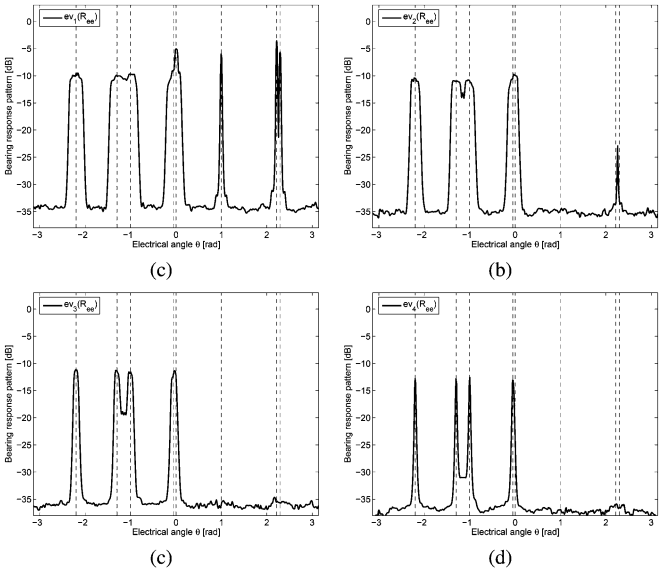

Fig. 8. Eigenvalue bearing response patterns: (a) $\mathrm{ev}_1(\mathbf{R}_{ee}(\theta))$, (b) $\mathrm{ev}_2(\mathbf{R}_{ee}(\theta))$, (c) $\mathrm{ev}_3(\mathbf{R}_{ee}(\theta))$, and (d) $\mathrm{ev}_4(\mathbf{R}_{ee}(\theta))$. The data covariance matrix $\mathbf{R}$ is estimated from $N = 1.5L = 192$ snapshots. Dashed vertical lines indicate true source locations. Going from negative to positive electrical angles in each plot the first four sources generate fluctuating waves with rank-4 covariances and the next four sources generate standing waves with rank-1 covariances.

are identical to those of Section V-A. Fig. 8(a)–(d) shows the plots of the eigenvalues of $\hat{\mathbf{R}}_{ee} = (\mathbf{\Psi}^H(\theta)\hat{\mathbf{R}}^{-1}\mathbf{\Psi}(\theta))^{-1}$ versus θ. Similar to the known data covariance case, the dominant eigenvalues of $\hat{\mathbf{R}}_{ee}$ resolve the rank-1 sources and the subdominant ones resolve the multirank sources. However, due to low sample support, loss of signal power is observed. This suggests that $\hat{\mathbf{R}}$ does not perfectly fit the four dimensional

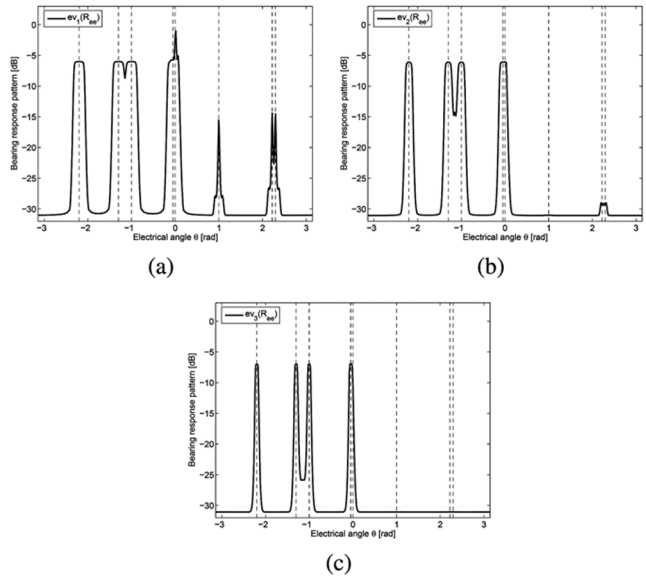

Fig. 9. Eigenvalue bearing response patterns: (a) $\mathrm{ev}_1(\mathbf{R}_{ee}(\theta))$, (b) $\mathrm{ev}_2(\mathbf{R}_{ee}(\theta))$, and (c) $\mathrm{ev}_3(\mathbf{R}_{ee}(\theta))$. The signal is modeled with a $\beta L = 3$ dimensional Slepian subspace and is mismatched to the actual $\beta L = 4$ dimensional Slepian signal subspace. Dashed vertical lines indicate true source locations. Going from negative to positive electrical angles in each plot the first four sources generate fluctuating waves with rank-4 covariances and the next four sources generate standing waves with rank-1 covariances.

signal subspace model, and brings us to the question of signal subspace mismatch.

C. Signal Subspace Mismatch

We now investigate the effect of signal subspace mismatch, where the Slepian subspace used in beamforming is different from the actual Slepian subspace used in generating the data. Fig. 9(a)–(c) shows the plots of the eigenvalues of $\mathbf{R}_{ee} = (\mathbf{\Psi}^H(\theta)\mathbf{R}^{-1}\mathbf{\Psi}(\theta))^{-1}$ versus θ, when $\mathbf{\Psi}(\theta)$ is taken to be the $\beta L = 3$ dimensional Slepian subspace instead of the four dimensional Slepian subspace used in generating the data. In this case, $\mathbf{R}_{ee}$ has three eigenvalues. As can be seen, the dominant eigenvalue of $\mathbf{R}_{ee}$ captures a very small fraction (-15 dB) of the power of the rank-1 sources at $\theta = 1$, $\theta = 2.22$, and $\theta = 2.29$ rad. At first it may appear that $\mathrm{ev}_1(\mathbf{R}_{ee})$ captures all the power of the rank-1 source at $\theta = 0$. However, the power at that location is due to leakage of power from the nearby multirank source, a result of signal subspace mismatch.

The subdominant eigenvalues of $\mathbf{R}_{ee}$, say $\mathrm{ev}_3(\mathbf{R}_{ee})$ and $\mathrm{ev}_2(\mathbf{R}_{ee})$ in Fig. 9(b) and (c), still resolve the multirank sources. This behavior may be explained using the GSC in Fig. 3. Roughly speaking, since here the dimension of the signal subspace is underestimated (three instead of four) the part of the signal that lies in the subspace spanned by the fourth Slepian basis vector, associated with $\beta = 4/L$, leaks through the bottom branch of the GSC. The Slepian basis vectors associated with $\beta = 3/L$ are different from those associated with $\beta = 4/L$. However, the three-dimensional Slepian subspace with $\beta = 3/L$ lies inside the four-dimensional Slepian subspace with $\beta = 4/L$. Therefore, when estimating the top branch from the bottom one and forming the error, the signal

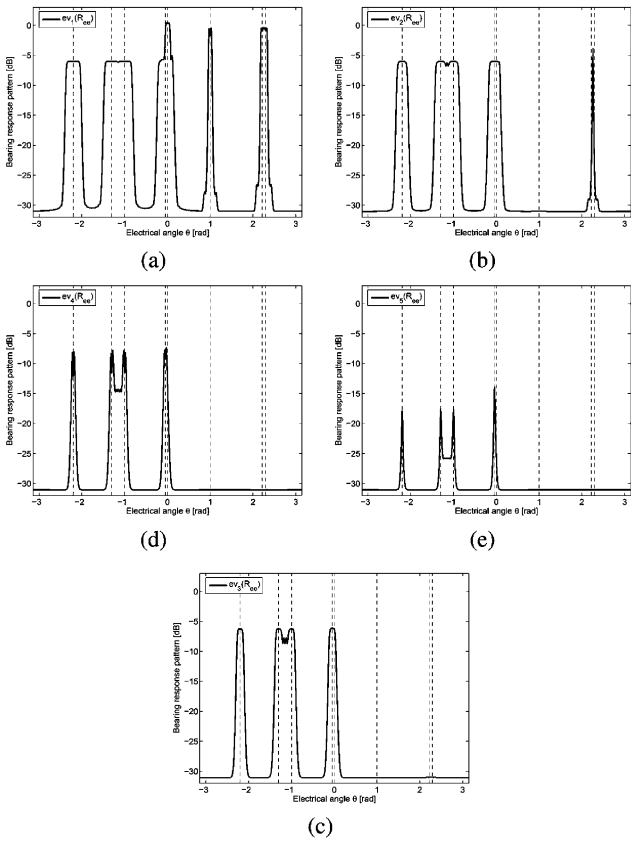

Fig. 10. Eigenvalue bearing response patterns: (a) $\mathrm{ev}_1(\mathbf{R}_{ee}(\theta))$, (b) $\mathrm{ev}_2(\mathbf{R}_{ee}(\theta))$, (c) $\mathrm{ev}_3(\mathbf{R}_{ee}(\theta))$, (d) $\mathrm{ev}_4(\mathbf{R}_{ee}(\theta))$, and (e) $\mathrm{ev}_5(\mathbf{R}_{ee}(\theta))$. The signal is modeled with a $\beta L = 5$ dimensional Slepian subspace and is mismatched to the actual $\beta L = 4$ dimensional Slepian signal subspace. Dashed vertical lines indicate true source locations. Going from negative to positive electrical angles in each plot the first four sources generate fluctuating waves with rank-4 covariances and the next four sources generate standing waves with rank-1 covariances.

components in the top branch that are correlated with those in the bottom branch are suppressed. The signal suppression can be more extreme for resolving rank-1 sources than multirank sources, because the power of a rank-4 source is equally distributed among four modes in the Slepian subspace. The power of a rank-1 source on the other hand is concentrated along one direction in the space and hence may be significantly reduced when the dimension of the signal subspace is underestimated.

Next we overestimate the signal subspace dimension by taking the signal subspace to be the $\beta L = 5$ dimensional Slepian subspace. Fig. 10(a)–(d) shows the eigenvalue bearing response patterns for this case, where $\mathbf{R}_{ee}$ has five eigenvalues. The multirank sources are again resolved by the subdominant eigenvalues of $\mathbf{R}_{ee}$. The rank-1 sources at $\theta = 0$ and $\theta = 1$ are resolved at almost full power with the most dominant eigenvalue $\mathrm{ev}_1(\mathbf{R}_{ee})$. However, the rank-1 sources at $\theta = 2.22$ and $\theta = 2.29$ rad are not fully resolved by $\mathrm{ev}_1(\mathbf{R}_{ee})$. Compared to the previous mismatch scenario, here the dominant eigenvalue of $\mathbf{R}_{ee}$ provides better "detectability" (larger power level) around the location of the rank-1 sources. Roughly speaking, since here the dimension of the signal subspace is overestimated the signal does not leak through the bottom branch of the GSC. However, the interfering sources are not as strongly suppressed as before, because less correlated interference passes through the bottom branch. This effect is evident in Fig. 10(b), where $\mathrm{ev}_2(\mathbf{R}_{ee}(\theta))$ peaks in the middle of the rank-1 sources located at $\theta = 2.22$ and $\theta = 2.29$ rad.

VI. Conclusion

In many practical imaging and beamforming problems the signature vector of the signal of interest is not perfectly known, but the subspace in which the signature vector lies is known or can be approximated. The unknown orientation of the signal in the subspace may stay fixed, in which case the signal has a rank-one but unknown covariance matrix, or it may change randomly from one realization to another, in which case the signal has a known multirank covariance matrix. We present a unified and systematic treatment of such signal subspace and signal covariance models and discuss their relevance in radar, sonar, wireless communications, and biomedical imaging.

We derive two multirank generalizations of the MVDR beamformer, namely matched direction and matched subspace beamformers, by introducing a data dependent constraint matrix that is designed to extract information from the error covariance matrix associated with a GSC. When the signal of interest is drawn from an unknown but fixed direction within a known multidimensional subspace, and has a rank-1 covariance matrix, it is the dominant eigenvalues of the error covariance matrix that resolve the signal. When the signal is randomly drawn from a known multidimensional subspace, and has a known multirank covariance matrix, it is the subdominant eigenvalues that resolve the signal. In the former case, the constraint matrix is chosen to select the dominant eigenvectors of the error covariance, while in the latter case it is chosen to select the subdominant eigenvectors. This leads to eigenvalue beamforming, where each eigenvalue beamformer extracts signal information from an orthogonal subspace mode, at a different resolution. Matched direction and matched subspace beamforming are diversity combining techniques, in which per mode (per subspace dimension) output powers of eigenvalue beamformers are diversity combined to produce an estimate of the signal power. As the fraction of the signal power captured by the multirank beamformer increases the angular resolution decreases.

Appendix

Let $\mathbf{A}$ and $\mathbf{B}$ be $p \times p$ matrices with eigenvalues $\mathrm{ev}_1(\mathbf{A}) \geq \cdots \geq \mathrm{ev}_p(\mathbf{A}) \geq 0$ and $\mathrm{ev}_1(\mathbf{B}) \geq \cdots \geq \mathrm{ev}_p(\mathbf{B}) \geq 0$, then [47, ch. 9]

$$\begin{aligned}\sum_{i=1}^{k} ev_{p-i+1}(\mathbf{A}) ev_i(\mathbf{B}) &\leq \sum_{i=1}^{k} ev_i(\mathbf{AB}) \\ &\leq \sum_{i=1}^{k} ev_i(\mathbf{A}) ev_i(\mathbf{B}), \quad \text{for } k = 1, 2, \ldots, p. \end{aligned} \tag{A.1}$$

Set $\mathbf{A} = \mathbf{\Lambda}$ and $\mathbf{B} = \mathbf{B}(\theta) = \mathbf{S}(\theta, \theta_o)$. Since $\mathbf{\Psi}^H(\theta)\mathbf{\Psi}(\theta_o)\mathbf{\Lambda}\mathbf{\Psi}^H(\theta_o)\mathbf{\Psi}(\theta)$, $\mathbf{\Lambda}\mathbf{\Psi}^H(\theta_o)\mathbf{\Psi}(\theta)\mathbf{\Psi}^H(\theta)\mathbf{\Psi}(\theta_o)$, and $\mathbf{\Lambda}\mathbf{S}(\theta, \theta_o)$ have equal eigenvalues and $\mathbf{\Lambda}$ does not vary with θ, it is easy to see that the shape of the rank-k matched subspace bearing response pattern

$\sum_{i=1}^{k} \mathrm{ev}_i(\mathbf{\Psi}^H(\theta)\mathbf{\Psi}(\theta_o)\mathbf{\Lambda}\mathbf{\Psi}(\theta_o)^H\mathbf{\Psi}(\theta)) + k\sigma_n^2$, associated with the diagonal but nonidentity $\mathbf{\Lambda}$, follows the shape of the rank-k matched subspace bearing pattern associated with $\mathbf{\Lambda} = (1/p)\mathbf{I}$. For exposition, let $p = 4$ and $k = 2$, corresponding to a rank-2 matched subspace beamformer. Then, we have

$$\begin{aligned} &\lambda_4 ev_1(\mathbf{B}(\theta)) + \lambda_3 ev_2(\mathbf{B}(\theta)) \\ &\quad \le ev_1(\mathbf{AB}(\theta)) + ev_2(\mathbf{AB}(\theta)) \\ &\quad \le \lambda_1 ev_1(\mathbf{B}(\theta)) + \lambda_2 ev_2(\mathbf{B}(\theta)). \end{aligned} \tag{A.2}$$

Since $\lambda_1 \ge \cdots \ge \lambda_4 > 0$ we can write

$$\begin{aligned} &2\lambda_4[ev_1(\mathbf{B}(\theta)) + ev_2(\mathbf{B}(\theta))] \\ &\quad \le ev_1(\mathbf{AB}(\theta)) + ev_2(\mathbf{AB}(\theta)) \\ &\quad \le 2\lambda_1[ev_1(\mathbf{B}(\theta)) + ev_2(\mathbf{B}(\theta))]. \end{aligned} \tag{A.3}$$

Since $\mathbf{\Lambda}$ does not vary with θ the inequality in (A.3), which holds for any θ, shows that the width of $\mathrm{ev}_1(\mathbf{AB}(\theta)) + \mathrm{ev}_2(\mathbf{AB}(\theta))$ around θ_o has to be less than or equal to the width of $\mathrm{ev}_1(\mathbf{B}(\theta)) + \mathrm{ev}_2(\mathbf{B}(\theta))$ around θ_o.

REFERENCES

[1] H. L. Van Trees, *Optimum Array Processing*. New York: Wiley-Interscience, 2002.

[2] H. Cox, "Resolving power and sensitivity to mismatch of optimum array processors," *J. Acoust. Soc. Amer.*, vol. 54, pp. 771–758, 1973.

[3] D. D. Feldman and L. J. Griffiths, "A projection approach to robust adaptive beamforming," *IEEE Trans. Signal Process*, vol. 42, no. 4, pp. 867–876, Apr. 1994.

[4] I. S. Reed, J. D. Mallett, and L. E. Brennan, "Rapid convergence rate in adaptive arrays," *IEEE Trans. Aerosp. Electron. Syst.*, vol. AES-10, pp. 853–863, Nov. 1974.

[5] M. Wax and Y. Anu, "Performance analysis of the minimum variance beamformer in the presence of steering vector errors," *IEEE Trans. Signal Process.*, vol. 44, no. 4, pp. 938–947, Apr. 1996.

[6] H. Cox, R. M. Zeskind, and M. H. Owen, "Robust adaptive beamforming," *IEEE Trans. Acoust., Speech, Signal Process*, vol. ASSP-35, no. 10, pp. 1365–1376, Oct. 1987.

[7] J. Li, P. Stoica, and Z. Wang, "On robust Capon beamforming and diagonal loading," *IEEE Trans. Signal Process.*, vol. 51, no. 7, pp. 1702–1715, Jul. 2003.

[8] R. G. Lorenz and S. P. Boyd, "Robust minimum variance beamforming," *IEEE Trans. Signal Process.*, vol. 53, no. 5, pp. 1684–1696, May 2005.

[9] S. A. Vorobyov, A. B. Gershman, and Z.-Q. Luo, "Robust adaptive beamforming using worst-case performance optimization: A solution to the signal mismatch problem," *IEEE Trans. Signal Process.*, vol. 51, no. 2, pp. 313–324, Feb. 2003.

[10] S. Shahbazpanahi, A. B. Gershman, Z. Luo, and K. M. Wong, "Robust adaptive beamforming for general-rank signal models," *IEEE Trans. Signal Process.*, vol. 51, no. 9, pp. 2257–2269, Sep. 2003.

[11] A. Weiss and B. Friedlander, "'Almost blind' signal estimation using second-order moments," *Proc. Inst. Elect. Eng., Radar, Sonar Navig.*, vol. 142, pp. 213–217, Oct. 1995.

[12] A. Weiss and B. Friedlander, "Comparison of signal estimation using calibrated and uncalibrated arrays," *IEEE Trans. Aerosp. Electron. Syst.*, vol. 33, no. 1, pp. 241–249, Jan. 1997.

[13] M. Viberg and A. Swindlehurst, "A Bayesian approach to auto-calibration for parametric array processing," *IEEE Trans. Signal Process.*, vol. 42, no. 12, pp. 3495–3507, Dec. 1994.

[14] A. Swindlehurst, "A maximum *a posteriori* approach to beamforming in the presence of calibration errors," in *Proc. IEEE Statistical Signal Array Processing (SSAP) Conf.*, Corfu, Greece, Jun. 1996, pp. 82–85.

[15] R. A. Monzingo and T. W. Miller, *Introduction to Adaptive Arrays*. New York: Wiley, 1980.

[16] K. L. Bell, Y. Ephraim, and H. L. Van Trees, "Bayesian approach to robust adaptive beamforming," *IEEE Trans. Signal Process.*, vol. 48, no. 2, pp. 386–398, Feb. 2000.

[17] L. C. Godara, "Error analysis of the optimal antenna array processors," *IEEE Trans. Aerosp. Electron. Syst.*, vol. AES-22, no. 4, pp. 395–409, Jul. 1986.

[18] J. Li and P. Stoica, *Robust Adaptive Beamforming*. New York: Wiley, 2005.

[19] H. Cox, "Sensitivity considerations in adaptive beamforming," in *Proc. NATO Advanced Study Inst. Signal Processing With Particular Reference to Underwater Acoust.*, Loughborough, U.K., Aug. 1972, pp. 619–645.

[20] B. D. Van Veen, W. van Drongelen, M. Yuchtman, and A. Suzuki, "Localization of brain electrical activity via linearly constrained minimum variance spatial filtering," *IEEE Trans. Biomed. Eng.*, vol. 44, no. 9, pp. 867–880, Sep. 1997.

[21] T.-C. Lui and B. D. Van Veen, "Multiple window based minimum variance spectrum estimation for multidimensional random fields," *IEEE Trans. Signal Process.*, vol. 40, no. 3, pp. 578–589, Mar. 1992.

[22] O. L. Frost, "An algorithm for linearly constrained adaptive array processing," *Proc. IEEE*, vol. 60, pp. 926–935, Aug. 1972.

[23] M. K. Tsatsanis and Z. Xu, "On minimum output energy CDMA receivers in the presence of multipath," in *Proc. 31st Conf. Inform. Sci. Systems (CISS)*, Baltimore, MD, Mar. 19–21, 1997, pp. 724–729.

[24] M. K. Tsatsanis and Z. Xu, "Performance analysis of minimum variance CDMA receivers," *IEEE Trans. Signal Process.*, vol. 46, no. 11, pp. 3014–3022, Nov. 1998.

[25] K. Sekihara and B. Scholz, "Generalized Wiener estimation of three-dimensional current distribution from biomagnetic measurements," in *Proc. 10th Int. Conf. Biomagnetism (Biomag)*, Baltimore, MD, Feb. 1996, pp. 338–341.

[26] L. J. Griffiths and C. W. Jim, "An alternative approach to linearly constrained adaptive beamforming," *IEEE Trans. Antennas Propag.*, vol. AP-30, no. 1, pp. 27–34, Jan. 1982.

[27] O. Besson, L. L. Scharf, and F. Vincent, "Matched direction detectors," in *Proc. IEEE Int. Conf. Acoust., Speech, Signal Process*, Mar. 2005, pp. iv/977–iv/980.

[28] O. Besson, L. L. Scharf, and F. Vincent, "Matched direction detectors and estimators for array processing with subspace steering vector uncertainties," *IEEE Trans. Signal Process.*, vol. 53, no. 12, pp. 4453–4463, Dec. 2005.

[29] O. Besson and L. L. Scharf, "CFAR matched direction detector," *IEEE Trans. Signal Process.*, vol. 54, no. 7, pp. 2840–2844, Jul. 2006.

[30] L. L. Scharf, *Statistical Signal Processing*. Reading, MA: Addison-Wesley, 1991, pp. 330–331.

[31] L. L. Scharf and B. Friedlander, "Matched subspace detectors," *IEEE Trans. Signal Process.*, vol. 42, no. 8, pp. 2146–2157, Aug. 1994.

[32] M. Lundberg, L. L. Scharf, and A. Pezeshki, "Multi-rank Capon beamforming," in *Conf. Rec. 38th Asilomar Conf. Signals, Syst., Comput.*, Nov. 2004, vol. 2, pp. 2335–2339.

[33] L. L. Scharf, A. Pezeshki, and M. Lundberg, "Multi-rank adaptive beamforming," in *Proc. 15th IEEE Signal Processing Workshop*, Bordeaux, France, Jul. 17–20, 2005, pp. 307–312.

[34] H. Cox, A. Pezeshki, L. L. Scharf, O. Besson, and H. Lai, "Multi-rank adaptive beamforming with linear and quadratic constraints," in *Conf. Rec. 39th Asilomar Conf. Signals, Syst., Comput.*, Pacific Grove, CA, Oct. 1, 2005, pp. 338–341.

[35] D. Slepian, "Prolate spheroidal wave functions, Fourier analysis and uncertainty—V: The discrete case," *Bell Syst. Tech. J.*, pp. 1371–1430, 1978.

[36] D. J. Thomson, "Spectrum estimation and harmonic analysis," *Proc. IEEE*, vol. 70, pp. 1055–1096, Sep. 1982.

[37] C. T. Mullis and L. L. Scharf, "Quadratic estimators of the power spectrum," in *Adv. Spectrum Estimation*, S. Haykin, Ed. : Prentice Hall, 1990, vol. 1, ch. 1, pp. 1–57.

[38] K. M. Buckley, "Spatial/spectral filtering with linearly-constrained minimum variance beamformers," *IEEE Trans. Acoust., Speach, Signal Process*, vol. ASSP-35, no. 3, pp. 249–266, Mar. 1987.

[39] T. Trump and B. Ottersten, "Estimation of nominal direction of arrival and angular spread using an array of sensors," *Signal Process.*, vol. 50, pp. 57–69, Apr. 1996.

[40] O. Besson and P. Stoica, "Decoupled estimation of DOA and angular spread for a spatially distributed source," *IEEE Trans. Signal Process.*, vol. 48, no. 7, pp. 1872–1882, Jul. 2000.

[41] A. Paulraj and T. Kailath, "Direction of arrival estimation by eigenstructure methods with imperfect spatial coherence of wavefronts," *J. Acoust. Soc. Amer.*, vol. 83, pp. 1034–1040, Mar. 1988.

[42] S. Baillet, J. C. Mosher, and R. M. Leahy, "Electromagnetic brain mapping," *IEEE Signal Process. Mag.*, vol. 18, no. 6, pp. 14–30, Nov. 2001.

[43] M. Scherg and D. Von Cramon, "Two bilateral sources of late AEP as identified by a spatiotemporal dipole model," *Electroencephalogr. Clin. Neurophysiol.*, vol. 62, pp. 32–44, 1985.

[44] G. Strang, *Linear Algebra and Its Applications*, 2nd ed. Orlando, FL: Academic, 1980.
[45] A. Pezeshki, L. L. Scharf, M. Lundberg, and E. K. P. Chong, "Constrained quadratic minimizations for signal processing and communications," in *Proc. 44th IEEE Conf. Decision Contr.*, Seville, Spain, Dec. 2005, pp. 7949–7953.
[46] G. H. Golub and C. F. Van Loan, *Matrix Computations*, 3rd ed. Baltimore, MD: The Johns Hopkins Univ. Press, 1996.
[47] A. W. Marshall and I. Olkin, *Inequalities: Theory of Majorization and Its Applications*. New York: Academic, 1979.

Ali Pezeshki (S'95–M'05) received the B.Sc. and M.Sc. degrees in electrical engineering from the University of Tehran, Tehran, Iran, in 1999 and 2001, respectively, and the Ph.D. degree in electrical engineering at Colorado State University, Ft. Collins, in 2004.

During 2005, he was a Postdoctoral Researcher with the Signal Processing and Communications Laboratory at Colorado State University. Since January 2006, he has been a Postdoctoral Research Associate with The Program in Applied and Computational Mathematics at Princeton University, Princeton, NJ. His research interests are in statistical signal processing and coding theory, as they apply to sensing, communications and data networking.

Barry D. Van Veen (S'81–M'86–SM'97–F'02) was born in Green Bay, WI. He received the B.S. degree from Michigan Technological University, Houghton, in 1983 and the Ph.D. degree from the University of Colorado, Boulder, in 1986, both in electrical engineering. He was an ONR Fellow while working on the Ph.D. degree.

In spring 1987, he was with the Department of Electrical and Computer Engineering at the University of Colorado—Boulder. Since August 1987, he has been with the Department of Electrical and Computer Engineering (ECE) at the University of Wisconsin–Madison, where he is currently a Professor. He coauthored, with S. Haykin, *Signals and Systems* (New York: Wiley, 1999 (1st ed.) and 2003 (2nd ed.)). His research interests include signal processing for sensor arrays and biomedical applications of signal processing.

Dr. Van Veen was a recipient of a 1989 Presidential Young Investigator Award from the National Science Foundation and a 1990 IEEE Signal Processing Society Paper Award. He served as an Associate Editor for the IEEE TRANSACTIONS ON SIGNAL PROCESSING and on the IEEE Signal Processing Society's Statistical Signal and Array Processing Technical Committee and the Sensor Array and Multichannel Technical Committee. He received the Holdridge Teaching Excellence Award from the ECE Department at the University of Wisconsin in 1997.

Louis L. Scharf (S'67–M'69–SM'77–F'86–LF'07) received the Ph.D. degree from the University of Washington, Seattle.

From 1971 to 1982, he served as Professor of electrical engineering and statistics at Colorado State University (CSU), Ft. Collins. From 1982 to 1985, he was Professor and Chairman of electrical and computer engineering at the University of Rhode Island, Kingston. From 1985 to 2000, he was Professor of electrical and computer engineering at the University of Colorado, Boulder. In January 2001, he rejoined CSU as Professor of electrical and computer engineering and statistics. He has held several visiting positions here and abroad, including the Ecole Superieure d'Electricité, Gif-sur-Yvette, France; Ecole Nationale Superieure des Télécommunications, Paris, France; EURECOM, Nice, Italy; the University of La Plata, La Plata, Argentina; Duke University, Durham, NC; the University of Wisconsin, Madison; and the University of Tromsø, Tromsø, Norway. His interests are in statistical signal processing, as it applies to adaptive radar, sonar, and wireless communication. His most important contributions to date are to invariance theories for detection and estimation; matched and adaptive subspace detectors and estimators for radar, sonar, and data communication; and canonical decompositions for reduced dimensional filtering and quantizing. His current interests are in rapidly adaptive receiver design for space-time and frequency-time signal processing in the wireless communication channel.

Prof. Scharf was Technical Program Chair for the 1980 IEEE International Conference on Acoustics, Speech, and Signal Processing (ICASSP), Denver, CO; Tutorials Chair for ICASSP 2001, Salt Lake City, UT; and Technical Program Chair for the Asilomar Conference on Signals, Systems, and Computers 2002. He is past-Chair of the Fellow Committee for the IEEE Signal Processing Society and serves on its Technical Committees for Theory and Methods and for Sensor Arrays and Multichannel Signal Processing. He has received numerous awards for his research contributions to statistical signal processing, including an IEEE Distinguished Lectureship, an IEEE Third Millennium Medal, and the Technical Achievement and Society Awards from the IEEE Signal Processing Society.

Henry Cox (S'61–M'64–SM'82–F'83–LF'01) received the B.S. degree in physics from the College of the Holy Cross, Worcester, MA, in 1959 and the Sc.D. degree in electrical engineering from Massachusetts Institute of Technology (MIT), Cambridge, in 1963.

He is currently a Senior Fellow at Lockheed Martin DoD Systems, Arlington, VA. He was Senior Vice President and Chief Technology Officer (CTO) of Orincon before the merger with Lockheed Martin in June 2003. Previously, he was Divisional Vice President of BBN Systems. During his carrier as a naval officer, he held a number of important research and development positions, retiring as Captain of the U.S. Navy. He was the Project Manager for the Undersea Surveillance Project, Division Director at Defense Advanced Research Projects Agency (DARPA), and Officer in Charge of the New London Laboratory of the Naval Underwater Systems Center. He is the author of more than 60 technical papers. His recent contributions include development and application of robust adaptive beamforming algorithms to large towed arrays, development of simplified techniques for matched field processing, pioneering work in bistatic active sonar, new processing methods for Doppler exploitation in active sonar, new techniques for passive ranging, and development of system approaches for passive distributed systems, shallow-water active sonar and offboard sensors. His interests include antisubmarine warfare, adaptive signal processing, antenna arrays, underwater acoustics, and sonar system design and analysis.

Dr. Cox is a Fellow of the Acoustical Society of America. He was awarded the Gold Medal of the American Society of Naval Engineers. He received the Distinguished Technical Achievement Award of the Ocean Engineering Society. He was elected to the National Academy of Engineering in 2002.

Magnus Lundberg Nordenvaad (M'07) was born in Luleå, Sweden, in 1973. He received the M.Sc. degree in computer science and engineering from Luleå University of Technology (LTU), Luleå, Sweden, in 1998 and the Ph.D. degree in signal processing from the School of Electrical and Computer Engineering, Chalmers University of Technology, Gothenburg, Sweden, in 2003.

He has held visiting positions at Purdue University, West Lafayette, IN, and Colorado State University, Ft. Collins. Currently, he is an Assistant Professor with the Department of Computer Science and Electrical Engineering, LTU, and holds a senior research position at the Swedish Defence Research Agency. His research interests lie in statistical signal processing and how it applies to digital communications, radar, sonar, process diagnostics and land-mine detection.

Dr. Lundberg has received several awards and grants for his research. These include the 1998 MD110 User-Group Award for the Best Master's Thesis in the telecommunications area in Sweden that year and a postdoctoral scholarship award from the Swedish Research Council.